SINGLE-ULTRAFINE-PARTICLE MASS SPECTROMETER DEVELOPMENT AND APPLICATION

A Thesis

by

STANISLAV Y. GLAGOLENKO

Submitted to the Office of Graduate Studies of
Texas A&M University
in partial fulfillment of the requirements for the degree of

MASTER OF SCIENCE

August 2004

Major Subject: Mechanical Engineering

SINGLE-ULTRAFINE-PARTICLE MASS SPECTROMETER

DEVELOPMENT AND APPLICATION

A Thesis

by

STANISLAV Y. GLAGOLENKO

Submitted to Texas A&M University
in partial fulfillment of the requirements
for the degree of

MASTER OF SCIENCE

Approved as to style and content by:

Denis Phares (Chair of Committee)	Nagamangala Anand (Member)
Don Collins (Member)	Dennis O'Neal (Head of Department)

August 2004

Major Subject: Mechanical Engineering

ABSTRACT

Single-Ultrafine-Particle Mass Spectrometer

Development and Application. (August 2004)

Stanislav Y. Glagolenko, Dipl.; M.S.,

Mendeleyev University of Chemical Technology of Russia

Chair of Advisory Committee: Dr. Denis Phares

A single-ultrafine-particle mass spectrometer was constructed and deployed for size-resolved ultrafine aerosol composition measurements during the winter of 2002-2003 in College Station, Texas. Three separate experiments were held between December and March with six week intervals. Almost 128,000 mass spectra, corresponding to particles with aerodynamic diameters between 35 and 300 nm, were collected and classified. Fifteen statistically significant classes were identified and are discussed in this paper. Nitrate, potassium, carbon, and silicon/silicon oxide were the most frequently observed ions. Nitrate was present in most of the particles, probably due to the agricultural activity in the vicinity of the sampling site. The nitrate detection frequency was found to be sensitive to the ambient temperature and relative humidity. Another particle class, identified as an amine, exhibited strong relative humidity dependence, appearing only during periods of low relative humidity. There is evidence that some of the detected particles originated from the large urban centers, and were coated with nitrate, sulfate, and organics during transport.

To my loving parents, wife Anna and son Grisha.

ACKNOWLEDGEMENTS

I wish to express my gratitude to Dr. Denis Phares for his advice and support. I sincerely appreciate his time and effort through the duration of my thesis project. I wish to thank Professor Don Collins for helpful advice and discussion. I wish to thank Dr. Nagamangala Anand for his counsel and support. I would also like to gratefully acknowledge Marc Gonin, Katrin Fuhrer, and Al Schultz of Ionwerks, Inc., and Rishiraj Das for fabricating the OrthoTOF mass spectrometer and coupling the OrthoTOF to the inlet. My work was supported by the Texas Air Research Center under project number 082TAM2018A and by the Texas A&M Center for Environmental and Rural Health.

TABLE OF CONTENTS

LIST OF FIGURES

FIGURE Page

LIST OF TABLES

INTRODUCTION

Aerosols are known to impact human health through direct transport into the respiratory system and the environment by participating in heterogeneous chemical reactions, serving as cloud condensation nuclei, and scattering light. All of these processes are sensitive to the size and chemical composition of the individual particles. Determining these properties in real time, one particle at a time, would aid in understanding the effect of aerosols on health and the environment. Presently, single-particle mass spectrometers are the most suited instruments to making these measurements, despite the presence of certain composition and size biases. A number of single-particle mass spectrometers with different operating principles were developed during the last decade. The PALMS [*Thompson et al.,* 2000] instrument measures the light scattered by particles to approximate their size and to trigger an ablation laser. The ATOFMS [*Gard et al.,* 1997], LAMPAS-2 [*Trimborn et al.,* 2000] and SPLAT [*Schneider et al.,* 2004] instruments use light scattering to detect particles, and the aerodynamic diameter is determined from the particle time of flight between two points. The main disadvantage of the optical techniques is that particles too small to be detected by light scattering (roughly, smaller than 200 nm in diameter) cannot be analyzed. To overcome this limitation, an aerodynamic focusing mechanism was implemented in the RSMS-II instrument design [*Mallina et al.,* 2000*; Phares et al.,* 2002]. All five instruments employ time-of-flight mass spectrometry for chemical analysis. These

---

This thesis follows the style and format of *Journal of Geophysical Research.*

single-particle mass spectrometers were successfully deployed for aerosol measurements in numerous laboratory experiments and field campaigns.

The ATOFMS instrument was deployed for the online ambient aerosol characterization during April/May, 1995, in Riverside, CA [*Noble and Prather,* 1996]. Both positive and negative sign spectra were collected. Number of different particle types was observed during this experiment including hydrocarbon, elemental carbon, organic/nitrate, organic/inorganic, inorganic oxides and marine aerosols. Being size resolved measurements done by the ATOFMS made it possible to study correlations between chemical speciation within the particle types and particle size. Later the same instrument was used for the real time characterization of the pyrotechnically derived aerosol particles in the troposphere [*Liu et al.,* 1997]. The ATOFMS demonstrated the ability for detection and monitoring of the aerosol particles emitted by a well-defined source in the atmosphere. During September 1996 continuous measurements of single particle size and composition were made at a network of urban air monitoring sites in southern California [*Hughes et al.,* 1999]. A continuous time distribution series of sodium-, ammonium-, nitrate-, and carbon-containing particles were acquired. Results of this study showed also that the reduction in diesel soot and elemental carbon emission in nineties lead to reduce of the aerosol mass loading in the 0.2-0.3 μm size range. The ATOFMS was involved into the marine aerosol transport and chemistry study in fall 1996/winter 1997 [*Noble and Prather,* 1997; *Gard et al.,* 1998]. During the 1997 Southern California Ozone Study [*Liu et al.,* 2000; *Pastor et al.,* 2003], the major particles types detected included organic carbon with amines, elemental carbon, organic

carbon, ammonium nitrate, sea salt, soil dust, and various metal-rich types. The ATOFMS determined time variations in nitrate-containing particles that correlated well with concurrent nitrate measurements. The ATOFMS was also deployed during the Indian Ocean Experiment (INDOEX) to study the aerosol content of the oceanic troposphere influenced by the seasonal circulation of the polluted continental air masses [*Guazzotti et al.,* 2000].

Majority of the marine aerosols analyzed at Cape Green, Tasmania during the ACE – I field experiment by the PALMS instrument contained some sea salt [*Murphy et al.,* 1997c, 1998b; *Middlebrook et al.,* 1998]. Most of the sea salt aerosol mass spectra included also detectable organic, iodine, bromine and phosphate peaks. Major fraction of the detected particles had relatively high sulfate content. The organic and sulfate peaks found to have positive trend which can be indication of the marine particle's aging process. Nitrate was mainly associated with the alkaline-earth metals. The PALMS instrument was used for chemical analysis of single aerosol particles larger than 0.3 μm in diameter during the Idaho Hill experiment [*Murphy and Thompson,* 1997ab]. Potassium, iron, and organics were the most frequently observed ions in the positive spectra of the detected particles, while sulfate, nitrate and organics were the most common peaks in the negative ion spectra. Aerosols analyzed by the airborne version of the PALMS instrument during a high altitude aerosol mission were dominated by sulfate and water mixed with organics and a variety inorganic matter, including meteoritic material [*Murphy et al.,* 1998a]. Same set up was used for size resolved characterization of the aerosol in the wakes of solid rocket engine during the ACCENT field campaigns

in 1999 and 2000 [*Cziczo et al.,* 2002]. The collected particles were typically composed of combustion products of the rocket fuel and catalyst including chlorine, aluminum, iron, calcium and some other metals. Presence of the characteristic nitrate and sulfate peaks in the ion spectra indicated that particles generated in the rocket engine reacted with the gaseous nitric acid and ambient sulfuric acid particles within a very short period of time.

The LAMPAS-2 instrument was used for characterization of aerosol in a rural area during the four week LACE 98 field campaign [*Trimborn et al.,* 2000, 2002]. Ten main classes observed by LAMPAS-2 included sea salt, elemental and biogenic carbon, exhaust products and mineral dust. The size distributions of the elemental carbon and biogenic soot classes were shifted to the submicron mode, while aged sea salt particles were present only in a large size range. Mineral dust particles were observed in a size range from 0.2 to 1.5 μm. The air parcel back trajectories were used in order to distinguish particles sources and study transport related changes in aerosol composition. Detection frequency of the selected particle classes was found to be dependent on the traveling path of the studied air parcel across the continent and the sea. Fraction of the carbon containing, exhaust and mineral particles was higher when air masses stayed over the continent for the longer period of time. The LAMPAS-2 instrument was deployed for identification of the diesel exhaust particles at an Autobahn, urban and rural location [*Vogt et al.,* 2003]. Number concentration of the elemental carbon and carbonaceous particles detected during was significantly higher at the Autobahn site than at the rural location.

The RSMS-II, ATOFMS, and PALMS instruments were operated together during the 1999 Atlanta Supersite Project [*Middlebrook et al.,* 2003*; Rhoads et al.,* 2003*; Liu et al.,* 2003]. The Aerodyne aerosol mass spectrometer (AMS) was also deployed during this campaign [*Jayne et al.,* 2000*; Jimenez et al.,* 2003]. That instrument provides more quantitative chemical analysis, but not on a single particle basis. The four primary classes detected by RSMS-II, ATOFMS, and PALMS were organic carbon/sulfate, sodium/potassium/sulfate, soot/hydrocarbon, and mineral [*Middlebrook et al.,* 2003]. Carbonaceous particles comprised the majority of ultrafine aerosols detected by the RSMS-II indicating the prevalence of local combustion sources.

The RSMS-II instrument was also deployed close to a large cluster of oil refineries and chemical plants during the 2000 Houston Supersite experiment [*Phares et al.,* 2003]. The aerosol detected by the instrument in this industrial area was dominated by potassium, silicon, carbon, sea salt and iron. Carbon and nitrate were the primary components detected by the improved third version of the instrument (RSMS III) during the Baltimore Supersite experiment [*Lake et al.,* 2003].

We have built and deployed a single-ultrafine-particle mass spectrometer (SUPMS) that uses a dynamic focusing lens inlet, similar to RSMS-II. The SUPMS sampled during the winter of 2002 - 2003 in College Station, Texas. In addition to the convenience of sampling from the Texas A&M University campus, the site is unique compared to the predominantly urban or remote settings of many field campaigns involving single-particle mass spectrometers. College Station is located in an active agricultural area in the eastern portion of Texas and within 200 miles of Houston, Dallas, Austin and San

Antonio (the closest city being Houston, 90 miles to the Southeast). The local climate in winter time is influenced by cold and dry continental airflow and the relatively warm and humid air masses coming from the Gulf of Mexico. It is expected that the ambient aerosol is affected by the local agricultural activity and by industrial plumes from the major urban centers.

Laser Desorption/Ionization of Aerosols

Thompson and Murphy [1993] studied laser-induced ion formation thresholds of aerosol particles in a vacuum. In this study the micron range particles of different sizes and composition were ionized by four ultraviolet and one CO_2 lasers (193 nm, 248 nm, 308 nm, 337nm and 10.6 μm respectively). The ion formation threshold was found to decrease with the decreasing wave length. Difference between the ion formation threshold and the plasma formation threshold was greater for smaller laser wavelengths which allowed better control of the ionization process. The following work showed that further reduction of the wavelength to 157 nm only moderately lowers ionization threshold for most of the particles [*Thompson et al.,* 1997]. Absorption coefficients at 157 nm are much higher than at longer wave lengths which make it difficult to transmit energy from laser to ion source efficiently. It was also noted that the mass spectra of the specific aerosols differ depending on the laser wavelength and energy that reaches the particle. The absolute ion signal intensity obtained from the identical particles can vary significantly because of the shot to shot variation of the laser beam intensity and the non uniform beam profile. Having important advantages over the infrared and vacuum-

ultraviolet lasers the ultra violet lasers meet well the requirements of the most online aerosol mass spectrometry applications.

Particle size has a direct effect on its ionization properties. Thompson et al., [1993, 1997] reported that energy required for complete ionization of the micro meter range particle by the ultraviolet laser beam was proportional to particle diameter. The absolute peak areas of positive ion spectra produced from the sodium and potassium chlorides were found to decrease slowly with particle size going down from 150 to 12 nm [*Carson et al.*, 1997]. Nevertheless ion yields per unit mass were higher in case of smaller particles. Kane and Johnston [2000, 2001] studying a size biases in the detection of the individual ultrafine particles showed that particles with diameter above 100 nm can be ablated with almost unity efficiency. Below this limit ablation efficiency was decreasing with decreasing particle size. Measured ionization thresholds for 40 nm particles were significantly higher than for particles above 80 nm.

Both positive and negative ion types are produced during a particle ablation process. Cationic materials are usually represented in positive spectra, while negative spectra give information on anionic materials. Negative ions were found to have higher ionization thresholds than positive ones which can be explained by a strong free electron yield [*Thompson et al.,* 1997]. Combination of positive and negative spectra provides a more complete description of particle's chemical composition.

It is possible to obtain detectable ion signals from most types of materials using the laser desorption/ionization technique [*Johnston et al.,* 2000]. Ablation properties of aerosols generally depend on their composition. On average, the ionization thresholds

for organic particles are higher then for inorganic ones. Pure sulfuric acid has a highest ion formation threshold among all studied inorganic particles and can be efficiently ionized only by the 157 nm radiation. Sulfuric acid particles containing inorganic or organic impurities can be ionized by the 193 nm radiation. As it is expected organic aerosols composed from unsaturated and aromatic molecules require significantly lower ionization energy than aliphatic molecules. Aliphatic molecules with longer hydrocarbon chain are usually more stable and have lower ablation efficiency for diameters below 100 nm. Typical spectrum produced by the organic compound contains carbon-hydrogen clusters ($C_xH_y^+$). Elemental carbon particles produce carbon ions ($C_n^{+/-}$) and hence can usually be distinguished from the organic carbon. Molecular ions are rarely observed in the organic particle spectra because of the intensive fragmentation of the ablated molecules. Degree of fragmentation of the organic molecules is proportional to the laser beam energy. Presence of the easily ionized impurity lowers overall ionization threshold of aerosol almost to the level of a pure minor component. The ablation efficiency of the nanosclale multicomponent particles depends on the concentration and usually lies between ablation efficiencies of the pure components [*Kane et al.,* 2000].

Aerodynamic Focusing

Thin plate orifices, nozzles and capillary are commonly used as continuum sources of the particle beams in the various aerosol characterization instruments. Israel and Friedlander [1967] studying mono-disperse aerosol beams generated by the converging nozzle found that the expansion angle, the intensity and the velocity of the beam

generated depends on the upstream pressure, particle size and nozzle geometry. It was noted in particular that the minimum expansion angle corresponds to certain upstream pressure value which decreasing with decreasing particle size. Dahneke and Flachsbart [1972] discussed possible applications of the particle beam focusing including aerosol size selection and size spectrometry. Schwartz and Andres [1976] developed theoretical model of the time-of-flight aerosol spectrometer. This technique is based on the variation of the velocities which particles of different size obtain during the carrier gas expansion though nozzle in to the vacuum. Subsequent numerical modeling done by Dahneke and Cheng [1979] showed that if particle radius is small enough compared to the gas mean free path throughout the supersonic nozzle jet flow only particles in a narrow size range can be sharply focused at a given location. Size of the focused particles can be varied by changing upstream pressure or focusing distance. Focusing point can be determined by the series of skimmers which can intercept larger and smaller particles. Nozzle shape found to have only a moderate effect on the particle beam geometry. Theoretical modeling done by Fernandez de la Mora and Riesco-Chueca [1988] showed that particles are focused depending on their Stokes number (St) defined with in the focusing nozzle:

$$St = \frac{\tau v}{d},$$

Where d is the focusing orifice diameter, ν is the flow velocity through the orifice, and τ is the particle relaxation time.

$$\tau = \frac{\rho_p D_p^2 C_c}{18\mu},$$

Where ρ_p is the particle density, D_p is the particle diameter, and μ is the gas viscosity. The Cunningham slip correction C_c can be written as a function of the Knudsen number (Kn):

$$C_c = 1 + Kn(1.257 + 0.4e^{-1.1/Kn}).$$

Knudsen number can be determined from the kinetic properties of the expanding gas:

$$Kn = \frac{2\lambda}{D_p},$$

$$\lambda = \frac{2\mu}{P\sqrt{8M/\pi RT}},$$

Where λ is the mean free path of the carrier gas, M is the molecular weight, R is the universal gas constant. P and T are the pressure and temperature of the flow in the orifice, which can be calculated using potential flow theory for the case of the one-dimensional isentropic choked flow.

Negative effects that influence aerosol focusing were discussed also by Fernandez de la Mora. Only particles which trajectories originated relatively close to the nozzle axis pass through focal point. Particles which trajectories originated farther from the centerline are not usually sharply focused due to the presence of the so called geometrical aberration. Defocusing caused by this phenomenon can me minimized by the appropriate aerodynamic design. Brownian motion of the carrier gas molecules disturbs linear trajectories of the particles in the free molecular region. It leads to the misalignment of the particle beam which expected to be stronger for smaller particles. The third negative effect is caused by the viscous boundary layer developed near the

nozzle walls. It is becoming more noticeable at lower Reynolds numbers restricting good focusing in such flow regime.

The aerodynamic focusing became an important technique which was utilized in number of instruments including the RSMS – II. In the early version of this instrument particles were size selected by the differential mobility analyzer (DMA) before injection into the mass spectrometer where they were ionized by the free firing laser [*Carson et al,* 1997]. To improve a particle transition rate a new inlet that transmits particles in a narrow size range and form high speed particle beam was introduced [*Mallina et al.,* 2000]. Working principle of the aerodynamic focusing inlet is illustrated on Figure 1.

Inlet consists of a low and a high pressure regions separated by a thing plate with an axisymmetric focusing orifice. As aerosols pass through the focusing orifice into a low pressure region they keep moving with the linear trajectories and are focused depending on the Stokes number determined within the thing plate orifice. Particles with the larger Stokes numbers cross centerline closer to the orifice. Particles with the optimum value of Stokes number cross centerline farther downstream and enter ionization region of a mass spectrometer through the series of gas skimmers. Those with smaller Stokes numbers don't cross centerline and are pumped out with the carrier gas molecules. Mean diameter of the transmitted particles can be chosen by varying an upstream inlet pressure or a focusing orifice diameter.

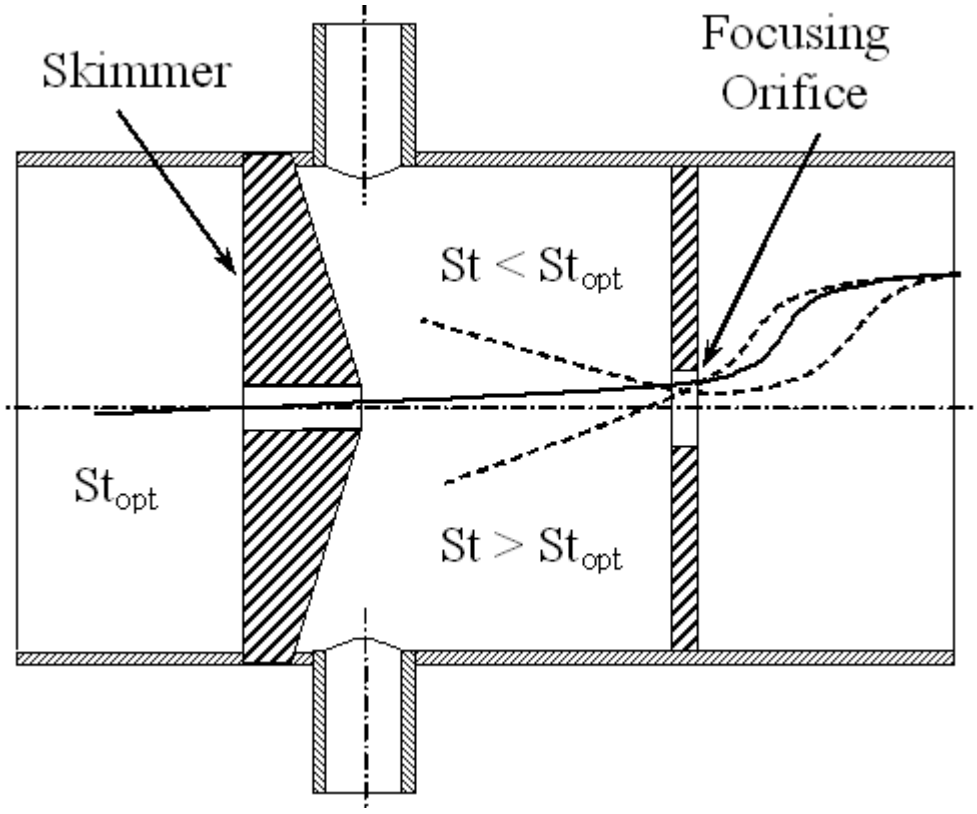

Figure 1. Working principle of aerodynamic focusing inlet.

INSTRUMENT

The single-ultrafine-particle mass spectrometer (SUPMS) used in the present study and depicted in Figure 2 is similar in operation to RSMS-II, but a number of modifications were made in order to make the instrument more compact and to improve resolution of an acquired spectra. The SUPMS employs a dynamic focusing inlet that transmits aerosol within a narrow aerodynamic size range to the mass spectrometer for subsequent desorption and ionization. The geometry and operation of the dynamic focusing inlet used in this study has been characterized previously [*Das and Phares,* 2004]. Aerosol enters the inlet through an automated multipositioning rotary valve (Valco Instruments Co.) which directs flow to one of ten critical orifices (O'Keefe Controls Co), ranging in diameter from 0.08 to 0.22 mm. The aerosol is then size selected by a focusing orifice and three downstream gas skimmers. The focusing orifice 3 mm in diameter is drilled in a 1 mm thick blank copper gasket. The gas skimmers were machined into cones with a 1 mm axial capillary. To provide an excellent inlet alignment wire EDM was used to drill the focusing orifice and the capillaries after assembly of the inlet. The inlet pressure, monitored by a Pirani pressure gauge (Edwards), varies between 2 and 28 Torr depending on the rotary valve position. The inlet pressure determines the aerodynamic size of the aerosol that is optimally transmitted to the mass spectrometer (see Table 1).

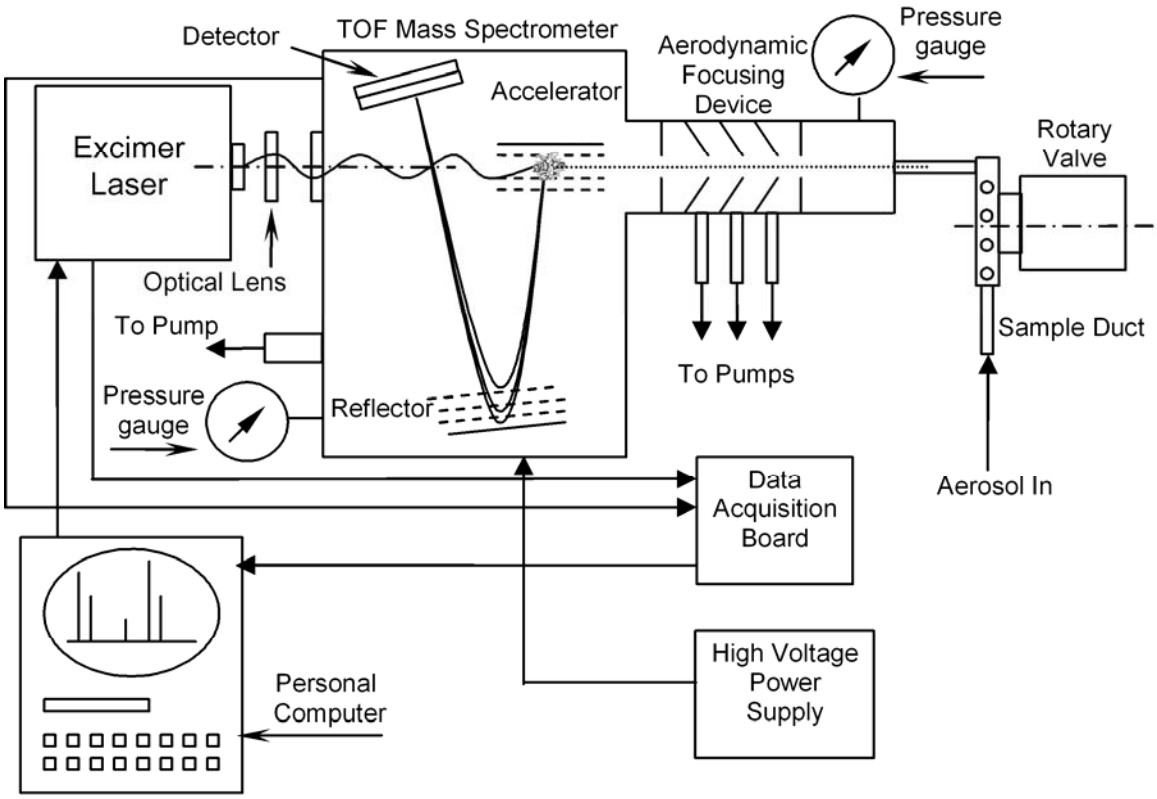

Figure 2. Schematic of single-ultrafine-particle mass spectrometer.

Table 1. Valve position, orifice diameter, upstream pressure and aerodynamic diameter of transmitted aerosol particles.

Valve Position	Orifice ID, mm	$P_{upstream}$, Torr	Particle Diameter, nm
1	0.08	2.4	30
2	0.09	4.8	50
3	0.10	5.5	85
4	0.11	6.5	110
5	0.13	10.0	130
6	0.14	12.0	170
7	0.16	14.0	200
8	0.18	19.0	230
9	0.20	23.0	270
10	0.22	28.0	300

Transmitted particles enter the ionization region of the time-of-flight mass spectrometer where they may be ablated by an EX-5 laser (GAM, Orlando, FL), a compact excimer laser that produces 5 mJ pulses at 193 nm with a repetition rate of up to 200 Hz. The laser beam is focused to a waist less than 1 mm in diameter that intercepts the particle beam produced by the focusing inlet. If a particle coincides with the laser beam in this volume, the particle ablates resulting in high energy plasma. Ions that are produced during this process are analyzed by a compact, high resolution reflectron mass spectrometer (Ionwerks, Inc.), pumped by a V250 turbo pump (Varian). Ions are accelerated in a high intensity electric field formed by an acceleration plate and series of wire screens. Voltage on the plate is 10000V; voltage on the front screen is 5000V. A high voltage supply is used to provide them with electric energy. Initially ions have broad range of speeds. Reflection plates similar in designs to the acceleration plates are used to improve resolution. Voltages on the reflection plate and screen are 6784V and 5000V respectively. Ions with higher initial energy penetrate deeper to the back plate of the reflector and have longer trajectories than same ions with lower kinetic energy. Therefore the time range in which ions of the same mass reach the detector is less for reflectrone mass spectrometer than for the linear mass spectrometer. Since molecular fragmentation is significant during laser ablation of ultrafine particles, the accelerator and reflectron voltages are set to maximize the peak resolution for the lighter ions ($m/z < 50$). Consequently, peaks corresponding to the heavier ions (particularly lead) are wider than a mass unit, making it difficult to resolve isotopic distributions. The peak resolution for $m/z < 50$ is greater than 100 (FWHM). The pressure within the mass spectrometer

controlled by the Active Ion Gauge (Edwards), varied between 10^{-9} and 10^{-6} Torr, depending on the inlet pressure. The detected ion signal is digitized by an Acqiris data acquisition system and processed and stored by a PC. In the present study, particles were classified based only on the resulting positive ion spectra. The instrument is fully automated and can run continuously for two days, after which only the laser requires maintenance. The entire SUPMS system was consolidated into a lightweight aluminum frame (60 cm x 100 cm x 200 cm).

INLET CALIBRATION

The SUPMS focusing inlet was calibrated using a technique described by Phares et al. [2002]. A TSI model 3076 atomizer was used as a source of the sodium chloride particles. Generated particles were then size selected by a high flow tandem differential mobility analyzer (TDMA) [*Gasparini et al.,* 2004]. Monodisperse particles of a known size and uniform composition were counted by the build in condensation particle counter (CPC). Well characterized aerosol flow was then injected into the SUPMS which was set to count particles without acquiring chemical composition information. Fraction of particles detected was assumed to be proportional to the particle transmission efficiency of the focusing inlet. The particle detection efficiency, PDE, for a given pressure can be found as:

$$\mathrm{PDE} = \frac{\mathrm{N_{SUPMS}}}{\mathrm{N_{CPC}}},$$

Where $\mathrm{N_{SUPMS}}$ is a number of particles detected by the SUPMS, and $\mathrm{N_{CPC}}$ is the number of particles counted by the CPC instrument.

To find particle size which corresponds to the highest transmission efficiency for chosen upstream inlet pressure the TDMA was stepping through the different particle sizes at a constant flow load. Particles counted by the SUPMS and CPC during 10 minutes periods for each particle size. This procedure was repeated twice for the upstream inlet pressure values 20 and 38 Torr. Normalized particle detection efficiencies were plotted as a function of the particle size (see Figure 3). The optimally transmitted particle diameter was determined from a maximum value of the particle detection

efficiency curve for each pressure. The dynamic focusing inlet selects particles based on the aerodynamic diameter which can be obtained in the free molecular limit by multiplying particle's density by the actual diameter measured by the TDMA. The results of the inlet calibration are presented on the on the Figure 4 where the optimally transmitted particle's aerodynamic diameters are plotted versus the corresponding upstream inlet pressure. As it could be seen from this figure the calibration data shows a good agreement with previous experiments and numerical modeling results. The optimally focused Stokes number was found to be close to 1.

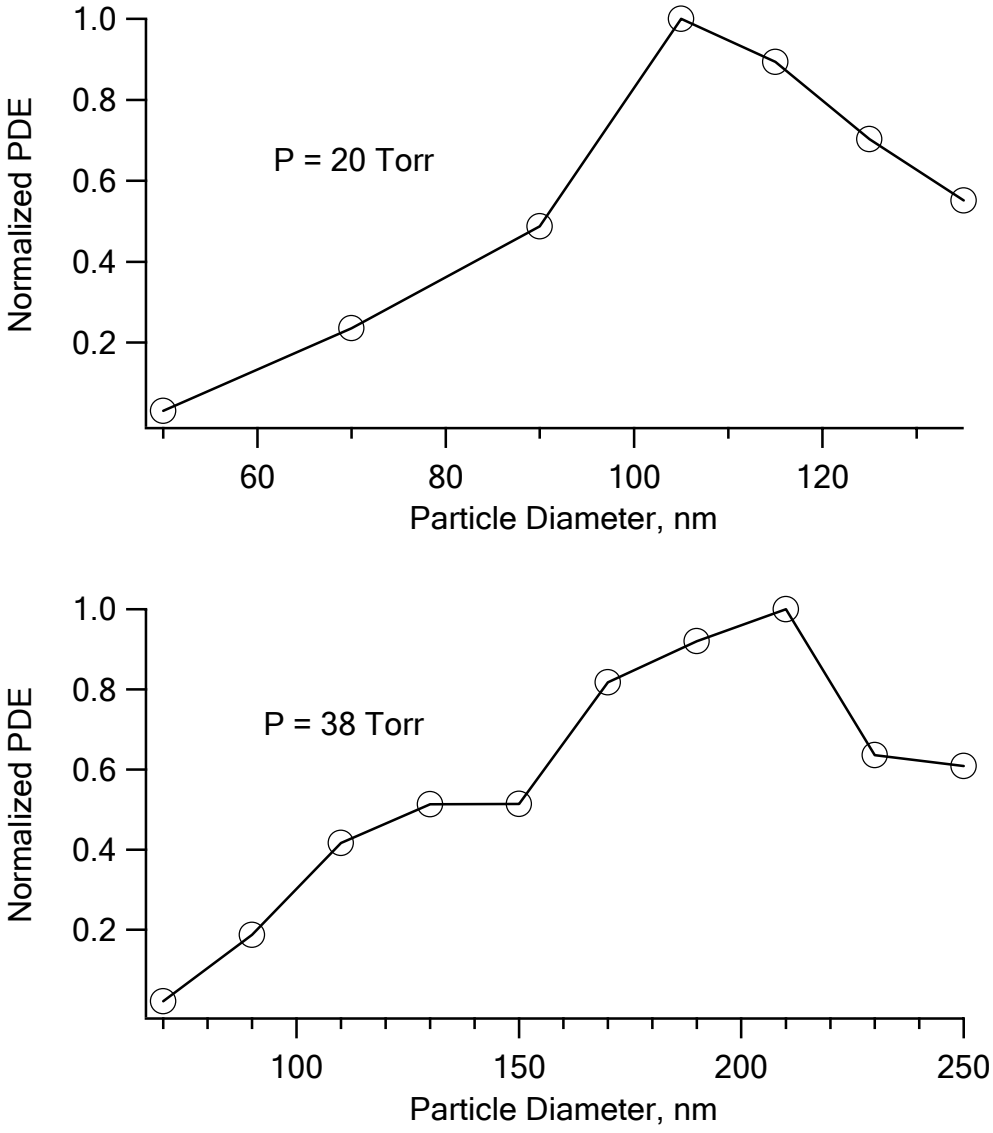

Figure 3. Normalized particle detection efficiencies of sodium chloride particles as a function of aerodynamic size.

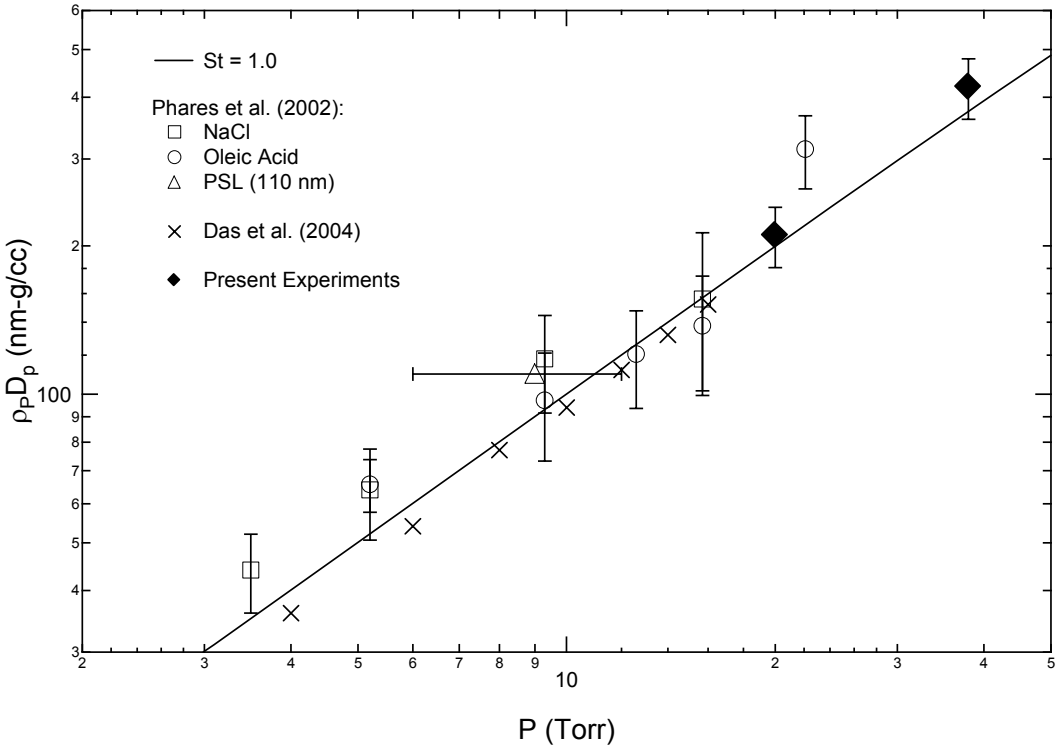

Figure 4. Inlet calibration curve.

DEPLOYMENT

During the winter of 2002-2003 the SUPMS was deployed in College Station, Texas to determine size-resolved chemical composition of the ambient ultrafine aerosol. Three separate experiments were held in December, January-February, and March (see Table 2). The city of College Station is located 90 miles northwest of Houston, 170 miles south of Dallas, and 130 miles northeast of Austin (see Figure 5). A distinctive feature of the local environment is the high level of agricultural activity, especially livestock farming. The ambient aerosol is expected to be influenced by local agricultural sources and distant industrial sources.

The instrument was placed on the tenth flour of the Oceanography & Meteorology building on the Texas A&M University campus. Aerosol was aspirated from outside the building directly into the SUPMS inlet through a quarter-inch stainless steel sampling tube. The multipositioning valve was set to change positions every two minutes. The instrument scanned through all 10 critical orifices every 20 minutes. The SUPMS was stopped for 3 minutes every 90 minutes for automated gas refilling of the excimer laser.

Table 2. Experiments schedule.

Experiment	Beginning Time, CST	Duration, hours	Particles Analyzed
I	12/06/2002 12:00	39	54873
II	01/30/2003 17:00	96	23102
III	03/07/2003 11:00	70	49875
	Total	175	127850

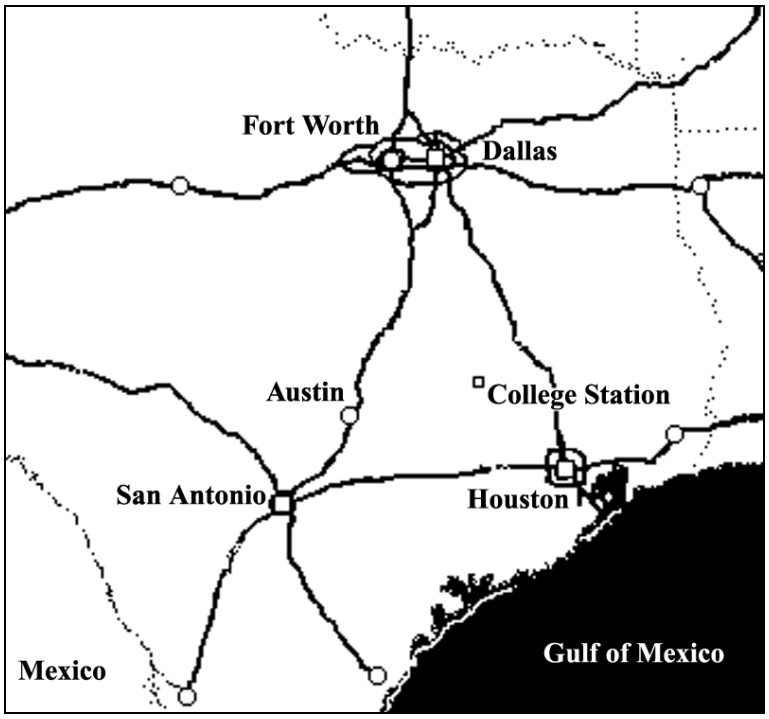

Figure 5. Location of the sampling site in College Station with respect to Houston, Dallas, Austin, and San Antonio.

Meteorology

The climate in the Bryan-College Station region is influenced by a predominant onshore airflow from the Gulf of Mexico and can be characterized as Subtropical Humid or Modified Marine. Seasonal intrusions of continental air masses can significantly vary moisture content in the atmosphere which is important for aerosol physics and transport. The present experiments included a variety of these weather conditions. The ambient temperature varied from 4° to 25°C and the relative humidity, from 40% to 100%.

Data Analysis

Almost 128,000 mass spectra were acquired during the three experiments. Automated particle classification was accomplished by the ART-2a algorithm. Details of the algorithm and its implementation were described by Phares *et al.* [2001]. In short, ART-2a groups similar mass spectra into classes facilitating subsequent chemical interpretation. Only classes containing more then 0.1% of the total detected particles during each experiment are presented in this paper. More than 40 particle classes were identified in each experiment and between 10 and 13 classes satisfied the 0.1% criterion in each case.

RESULTS

The results from all three experiments are summarized in Table 3. Details of each class are depicted in Figures 6 – 11 and 13 - 23**.** Each of these figures includes the mass spectrum averaged over each aerosol class, wind roses representing the detection frequency of each class as a function of wind direction for the first, second and third experiments (labeled "1", "2", and "3") and size distribution plots (also labeled accordingly). The size distribution plots are represented as a percentage of totals. Although the size distributions do not necessarily represent the real ambient aerosol size distribution due to size and composition detection biases [*Kane and Johnson,* 2000*; Phares et al.,* 2001], the size distribution of one class may be compared between experiments and to previous results. Finally, the lowest row of the figures displays the detection frequency of the class as a function of time. Each time trace, plotted as normalized hit rate, was normalized with respect to its Euclidian norm to facilitate comparison between experiments.

Table 3. Major particle classes identified during winter 2002-2003 experiments.

	Class Label	Percent of Total		
		I	II	III
1	Potassium	6.38	13.29	20.41
2	Carbon/Potassium	-	-	5.08
3	Carbon	10.30	4.34	26.34
4	Nitrate	68.41	26.40	17.97
5	Potassium/Nitrate	12.32	16.54	1.08
6	Carbon/Nitrate	–	–	23.2
7	Vanadium	0.70	0.54	0.14
8	Iron	0.4	0.33	0.73
9	Sea Salt	0.78	1.35	1.13
10	Silicon/Silicon Oxide	0.17	22.85	0.11
11	Calcium	0.13	–	–
12	Aluminum	-	0.22	0.167
13	Lead	0.13	–	–
14	Amine 1	–	1.53	–
15	Amine 2	0.29	2.59	1.16

Potassium and Carbon

Figures 6, 7, and 8 summarize three particle classes that exhibit varying relative amounts of carbon and potassium. Results from previous field campaigns [*Rhoads et al.,* 2003*; Phares et al.,* 2003] in urban settings include high detection rates of carbon and potassium. During the Houston study [*Phares et al.,* 2003], potassium was the most frequently observed particle class (comprising 31% of all detected particles). In the present study, the potassium particle class depicted in Figure 6 comprised 6% of the detected particles in December and increased steadily to over 20% in March. The small carbon peak (C^+) in the mass spectrum in Figure 6 suggests that either the particles were coated with organics or that at least some of the particles originated in the burning of biomass. Figure 7 summarizes results for a similar particle class that appears to be composed of a higher percentage of carbon, and is thus labeled as a "carbon/potassium" mixture. The main motivation for not grouping this class with the previous one is that the mixture was only detected in March during experiment 3. These particles likely resulted from biomass burning.

Figure 8 summarizes a class typified by clusters of carbon, as large as C_8^+, with a small amount of potassium. The high ionization efficiency of potassium suggests that potassium is present in these particles only in trace amounts. The carbon class comprises 15.5% of total particles detected. These particles were the most abundant class during the March experiment.

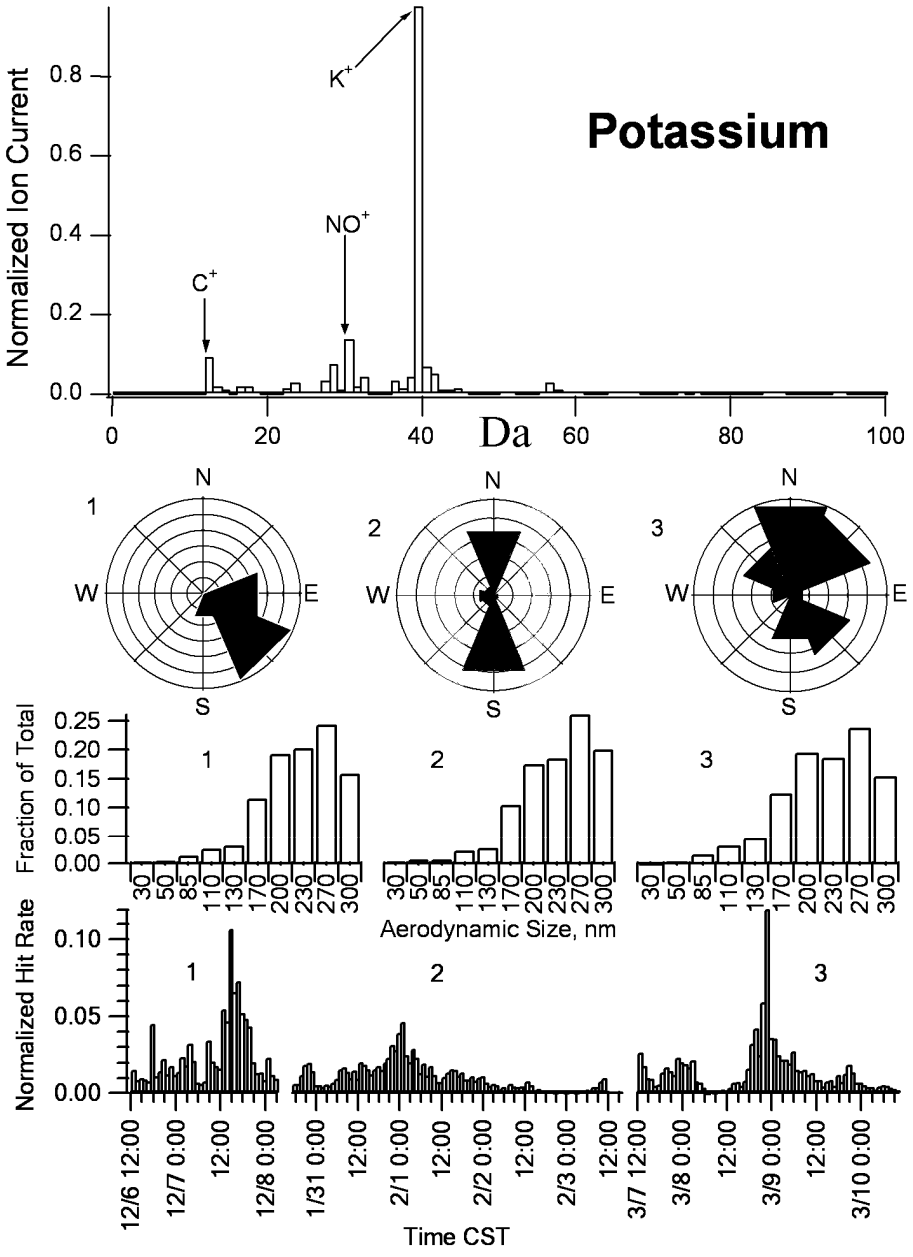

Figure 6. Statistics summary for potassium compound class. The mass spectrum represents the average for particles comprising this class. The wind roses plot hit rate frequency as a function of wind direction. The presented size distributions are uncorrected and are determined directly from the hit rate of the instrument. The histogram bars within size bin represent the fraction of total particles within the class detected during each experiment. Each time trace, plotted as normalized hit rate, was normalized with respect to its Euclidian norm to facilitate comparison between experiments.

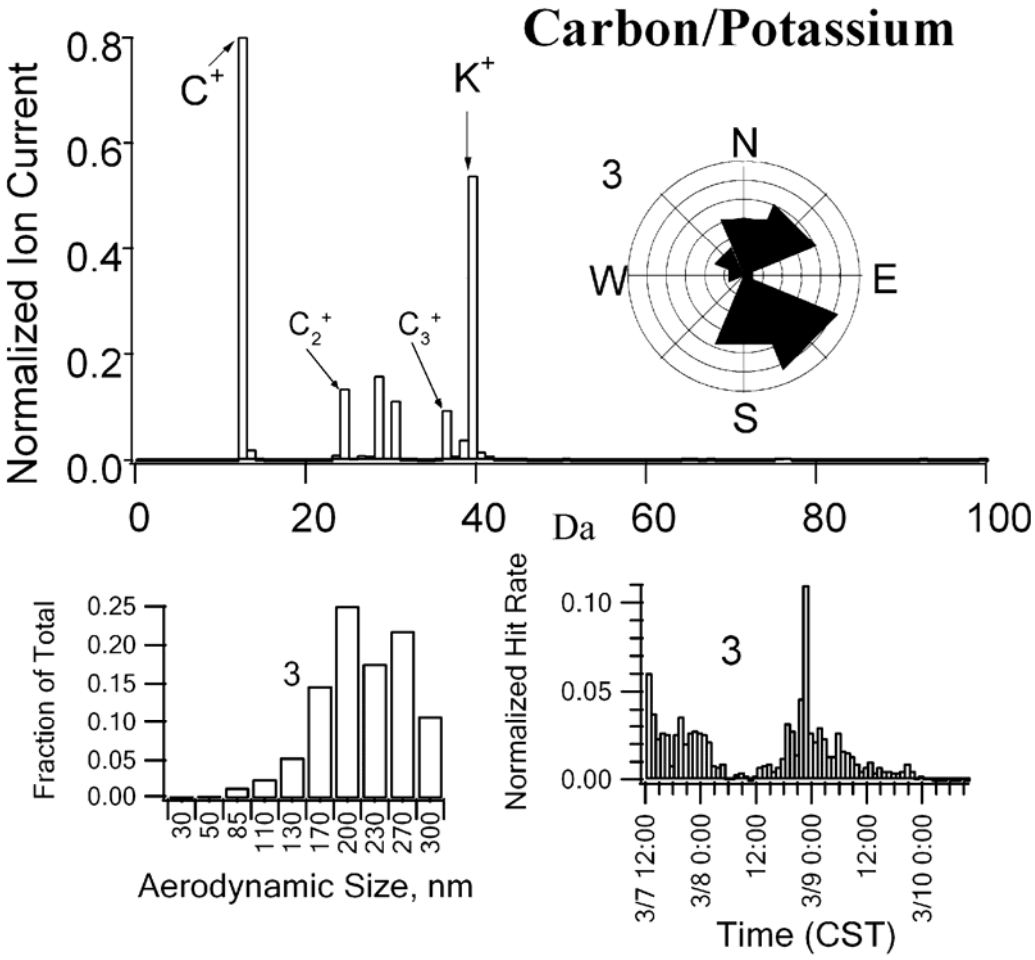

Figure 7. Statistics summary for carbon/potassium compound class.

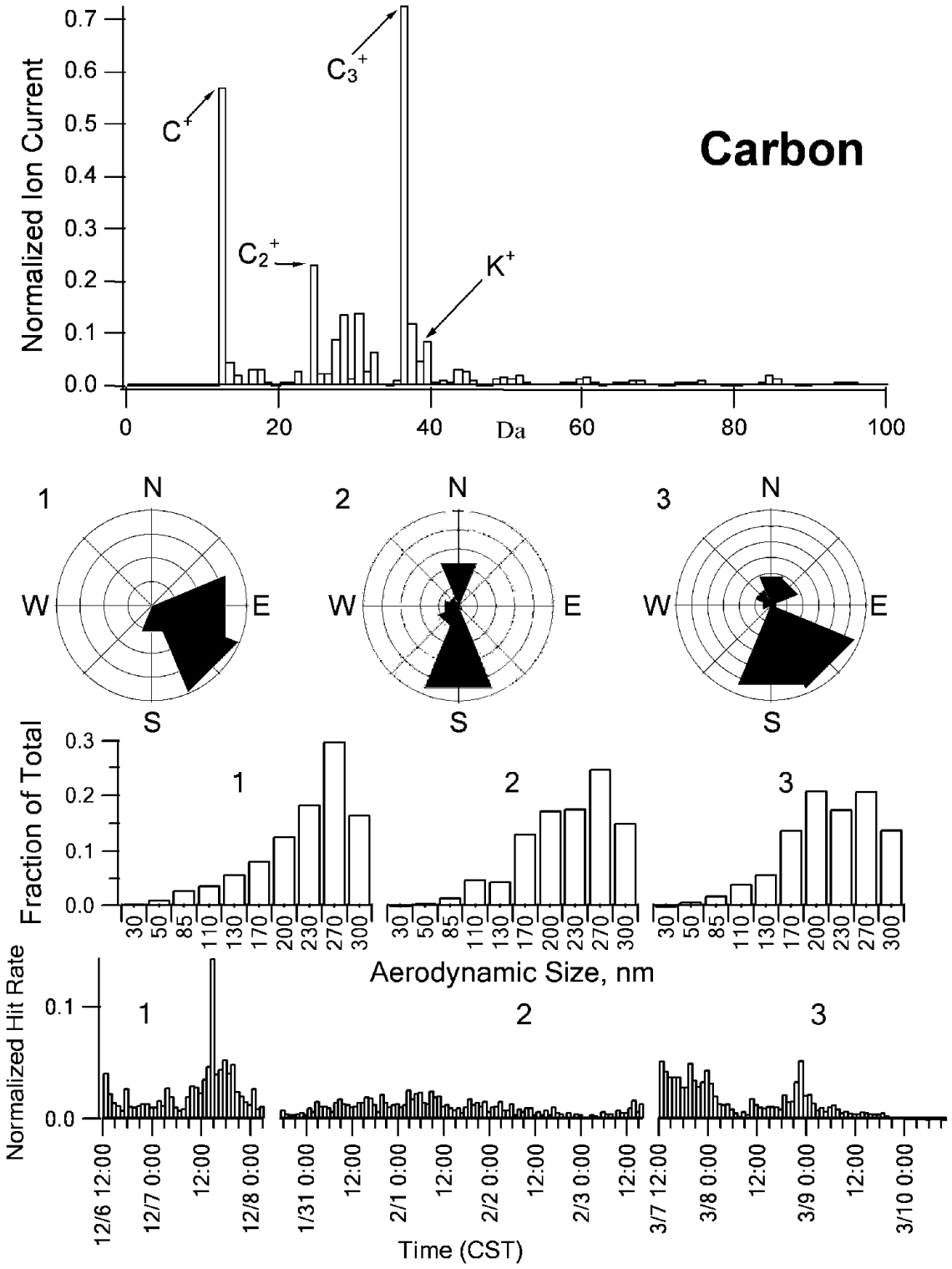

Figure 8. Statistics summary for carbon compound class.

High Nitrate Content Classes

Figures 9, 10, and 11 summarize three particle classes that feature a large nitrate peak (NO^+). The three classes, labeled "nitrate", "potassium/nitrate", and "carbon/nitrate", exhibit similar time, wind, and, size distributions and collectively represent the most commonly observed class throughout the sampling period. The high abundance of nitrate aerosol may be attributed to the agricultural activity in the vicinity, especially livestock farming which is accompanied by ammonia emission [*Misselbrook et al*., 2000].

The potassium/nitrate particles probably originated from biomass burning and subsequently reacted with nitric acid present in the atmosphere. The carbon/nitrate class resembles the carbon class except for the much higher nitrate peak. Particles in the carbon/nitrate class were detected in significant amounts only in March. The fact that these particles were not grouped with the carbon class is validated by their appearance under specific ambient conditions. For example, Figure 12 demonstrates that, unlike the carbon and potassium particles, the nitrate classes appear only during periods of lower temperatures and higher relative humidities during the March experiment. *Weber et al.* [2001] observed similar diurnal variation in the nitrate-containing aerosols using a particle-into-liquid collector. Nitrate particles detected by the SUPMS could have originated through the reaction of gaseous ammonia and nitric acid:

$$NH_3(g) + HNO_3(g) \Leftrightarrow NH_4NO_3(s).$$

The dissociation constant (K) and deliquescence relative humidity (DRH) of solid ammonia nitrate may be calculated using thermodynamic extrapolation formulas [*Stelson and Seinfeld*, 1982]:

$$\ln(DRH) = \frac{723.7}{T} + 1.7037,$$

$$\ln(K) = 84.6 - \frac{24220}{T} - 6.1\ln\left(\frac{T}{298}\right).$$

The dissociation constant, K, and the difference between the relative humidity and the deliquescence relative humidity of ammonium nitrate, (RH-DRH), throughout the March experiment are also depicted in Figure 12. According to these plots, the nitrate classes were observed when the dissociation constant was relatively low and only if the relative humidity was greater than the deliquescence relative humidity. This suggests that the detected particles were in the liquid phase, although the presence of an organic film may result in a higher deliquescence relative humidity. The relative absence of nitrate aerosol during the higher temperature periods may be explained by the increase in the dissociation constant.

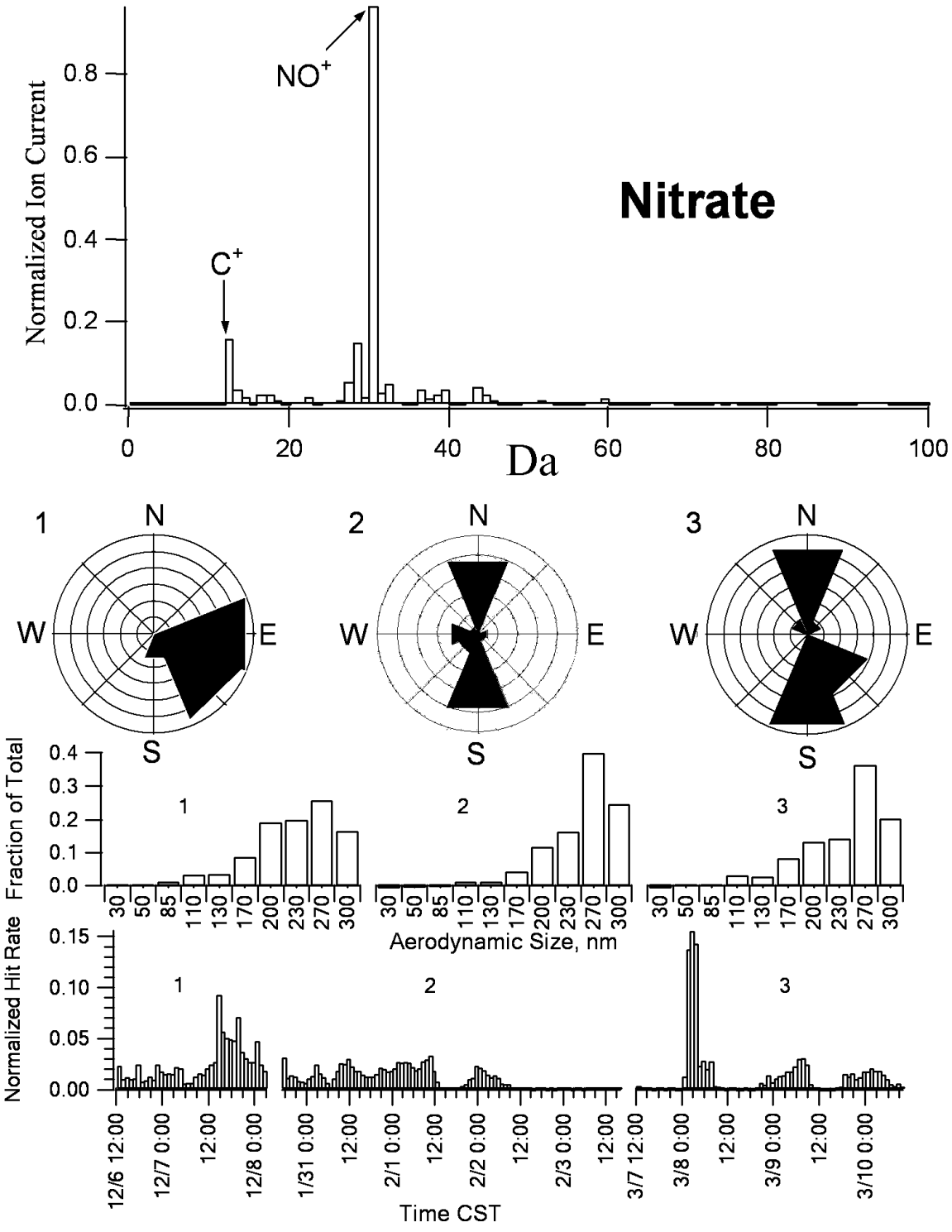

Figure 9. Statistics summary for nitrate compound class.

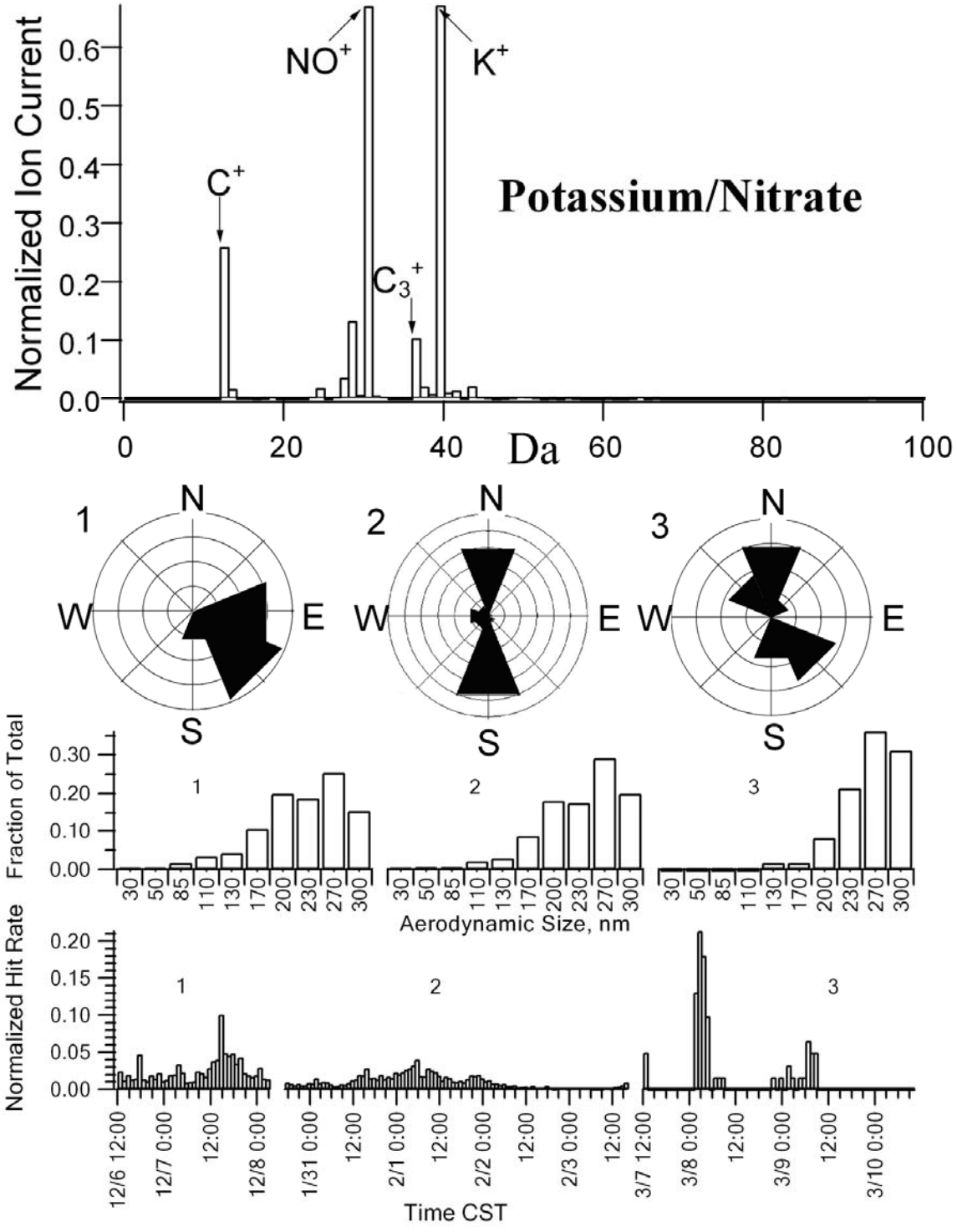

Figure 10. Statistics summary for potassium/nitrate compound class.

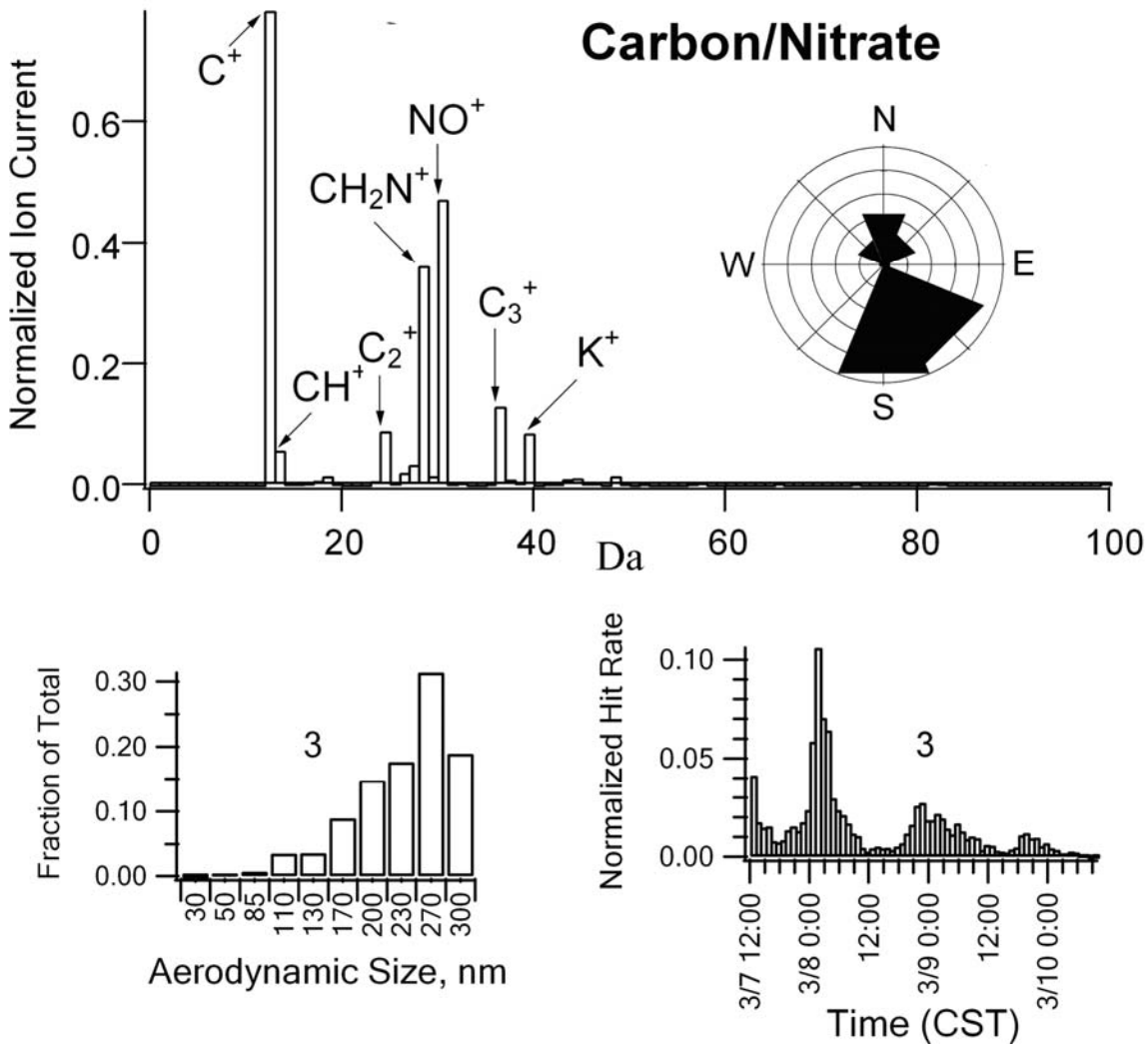

Figure 11. Statistics summary for carbon/nitrate compound class.

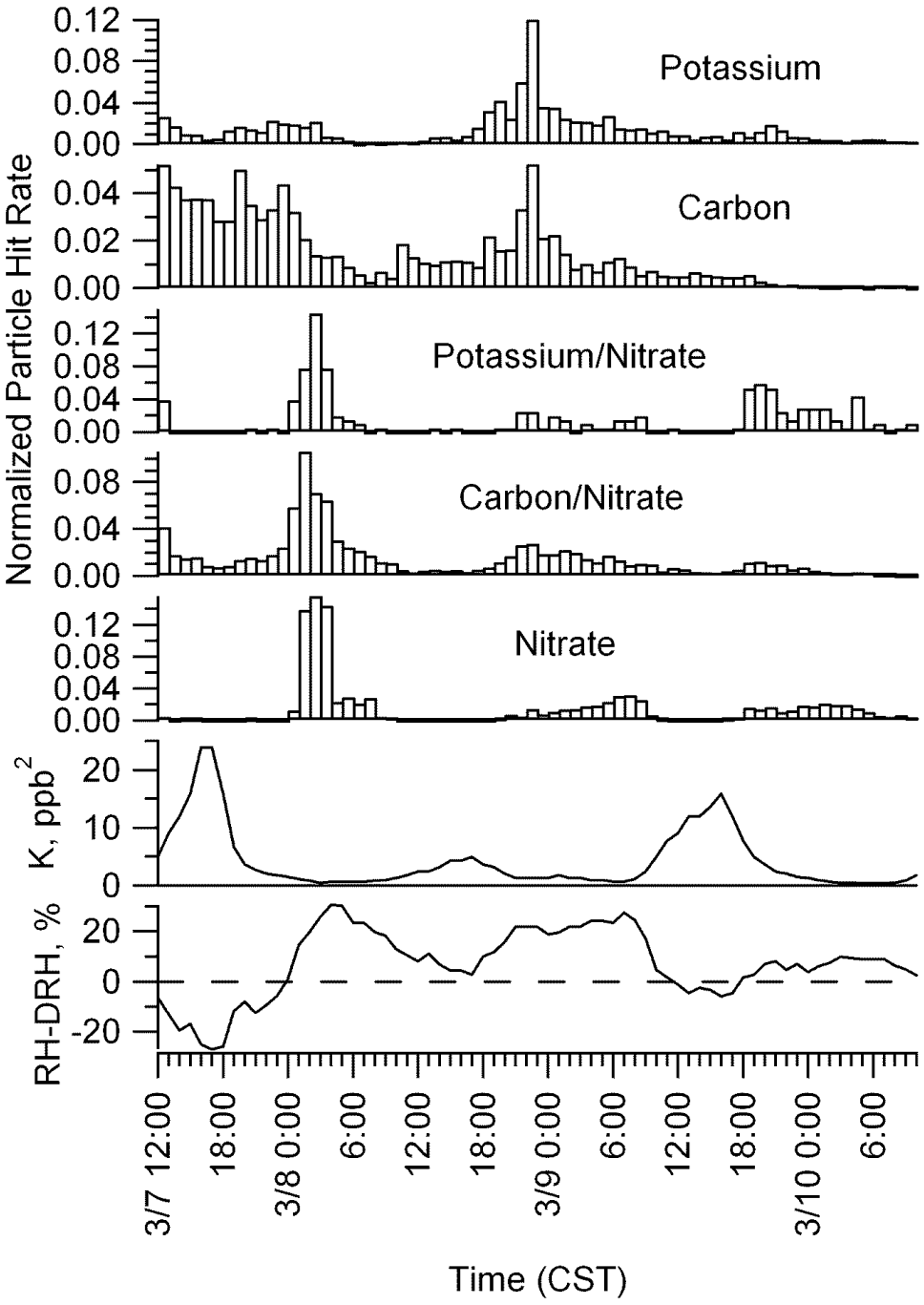

Figure 12. Nitrate, carbon/nitrate, potassium/nitrate, carbon, potassium aerosol classes detection frequencies time distributions and relative humidity and ammonia nitrate deliquescence relative humidity difference (RH-DRH) time variation for March experiment.

Vanadium

Vanadium (Figure 13) is usually released into the atmosphere during thermal cracking of crude oil and heavy fuel oil combustion. This class was previously detected prevalently during the 2000 Houston SuperSite experiment within the vicinity of a large number of oil refineries [*Phares et. all*, 2003]. The current experiments indicate that vanadium-containing aerosol from the South, Southeast, or east and could have originated from the same sources in Houston. In contrast to that study, the mean aerodynamic diameter of vanadium particles measured in College Station lies above 200 nm. This may be attributed to the presence of nitrate (evidenced by NO^+ at 30 Da) coating at the surface of the particles during transport.

Iron

Iron is easily recognized by the primary peak at 56 Da in the particle class summarized in Figure 14. This class comprised only 0.52% of the total particles analyzed. No strong wind direction dependence was observed, indicating that the particles were probably emitted by a distant source or multiple sources. Three possible sources of iron containing particles are mineral dust [*Zhang et al.,* 1998], coal combustion [*Smith et al.,* 1998] and pig iron/steel production processes [*Weinberg,* 1999].

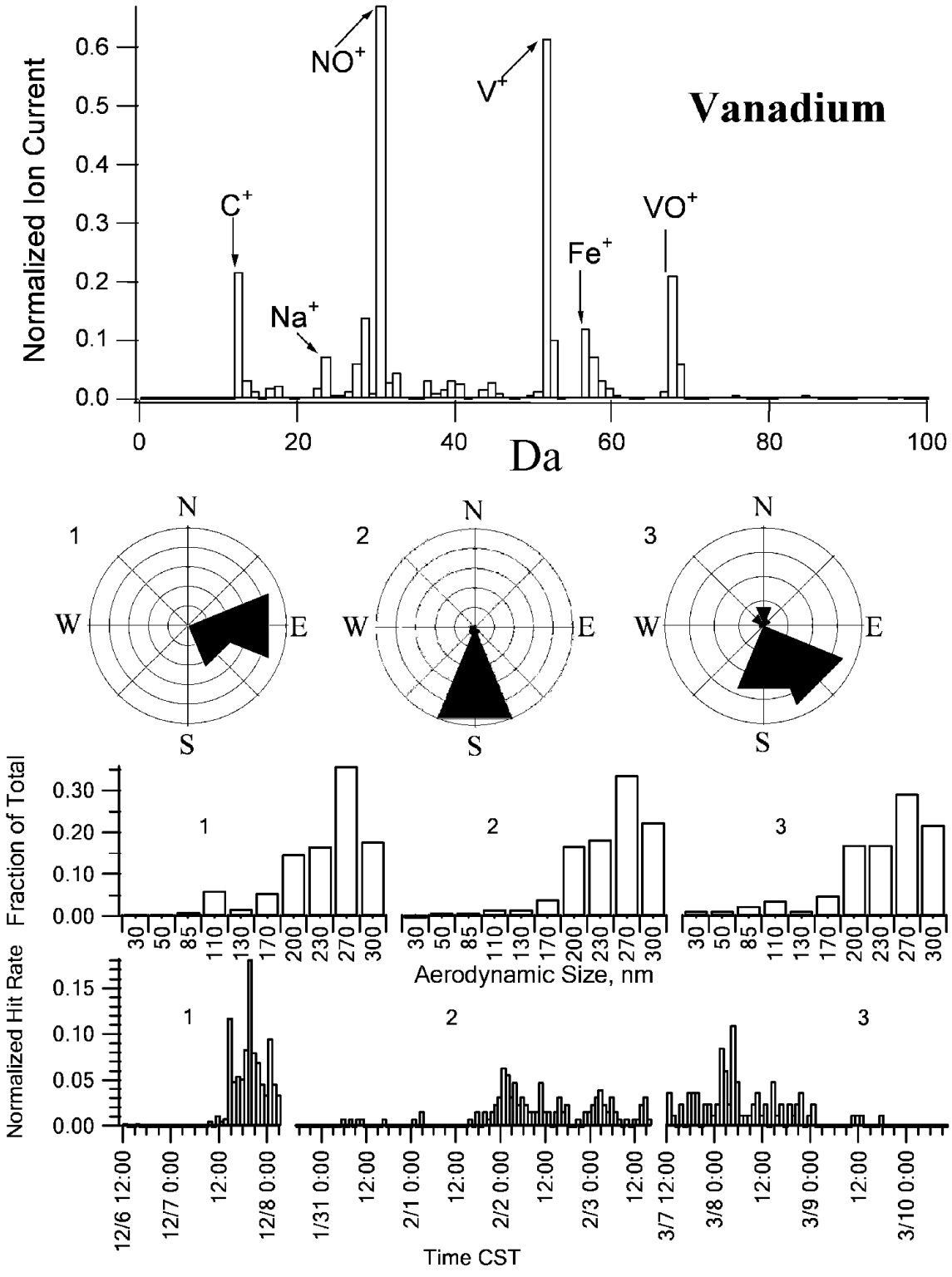

Figure 13. Statistics summary for vanadium compound class.

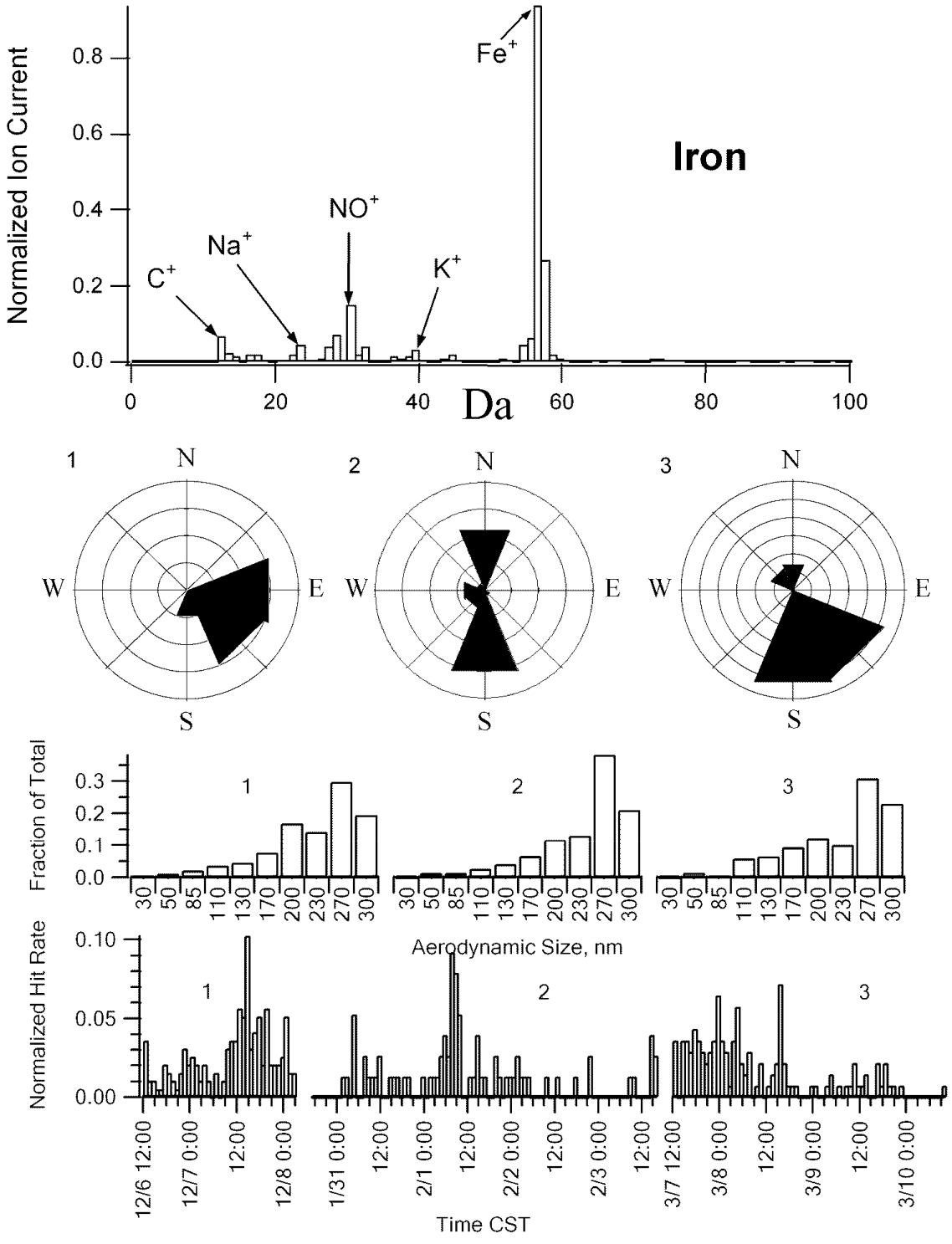

Figure 14. Statistics summary for iron compound class.

Sea Salt

Sea salt, typified by peaks corresponding to sodium and potassium [*Phares et al.,* 2003], comprised 1.02% of the detected particles (see Figure 15). The presence of the NO^+ peak in the ion spectra may have resulted from nitrate coating the surface of the particles or from reaction of Na/KCl with gaseous HNO_3 resulting in partial substitution of chloride with nitrate [*Gard et al.,* 1998]. We do not observe a peak corresponding to $Na_2NO_3^+$, as reported by *Gard et al.* [1998]; nor was this peak observed by RSMS-II in the sea salt particles detected during the Houston experiment. We note, however, that the ablation and ionization of ultrafine particles results in more ion fragmentation than for supermicron particles. Sea salt particles were generally detected from the southeast, but in January nearly half of sodium/potassium particles were transported from the North. This can be explained from back trajectories obtained from the HYSPLIT4 model [*Draxler*, 1988] showing a large recirculation of the air mass over Texas during that time (see Figure 16).

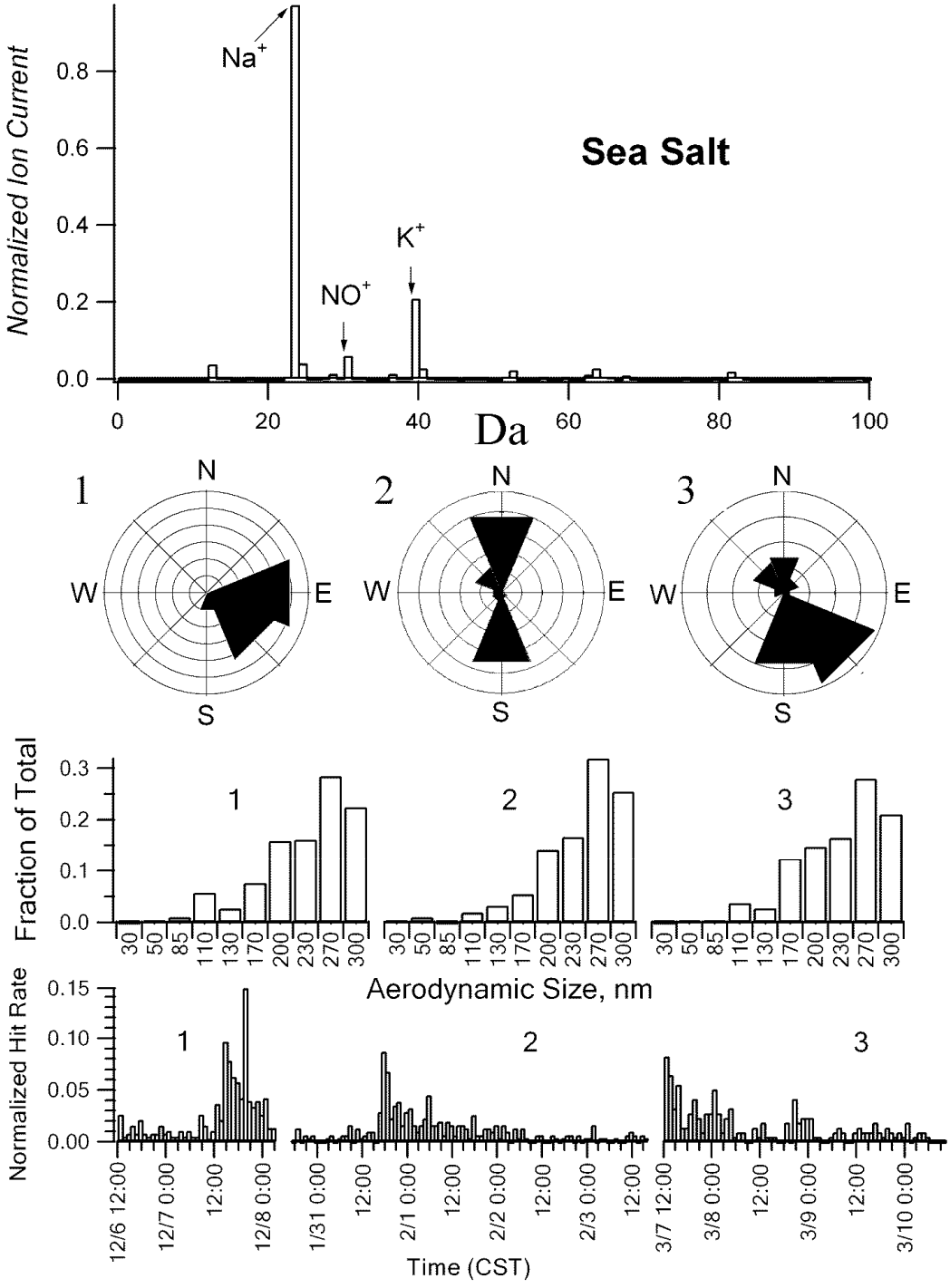

Figure 15. Statistics summary for sea salt class.

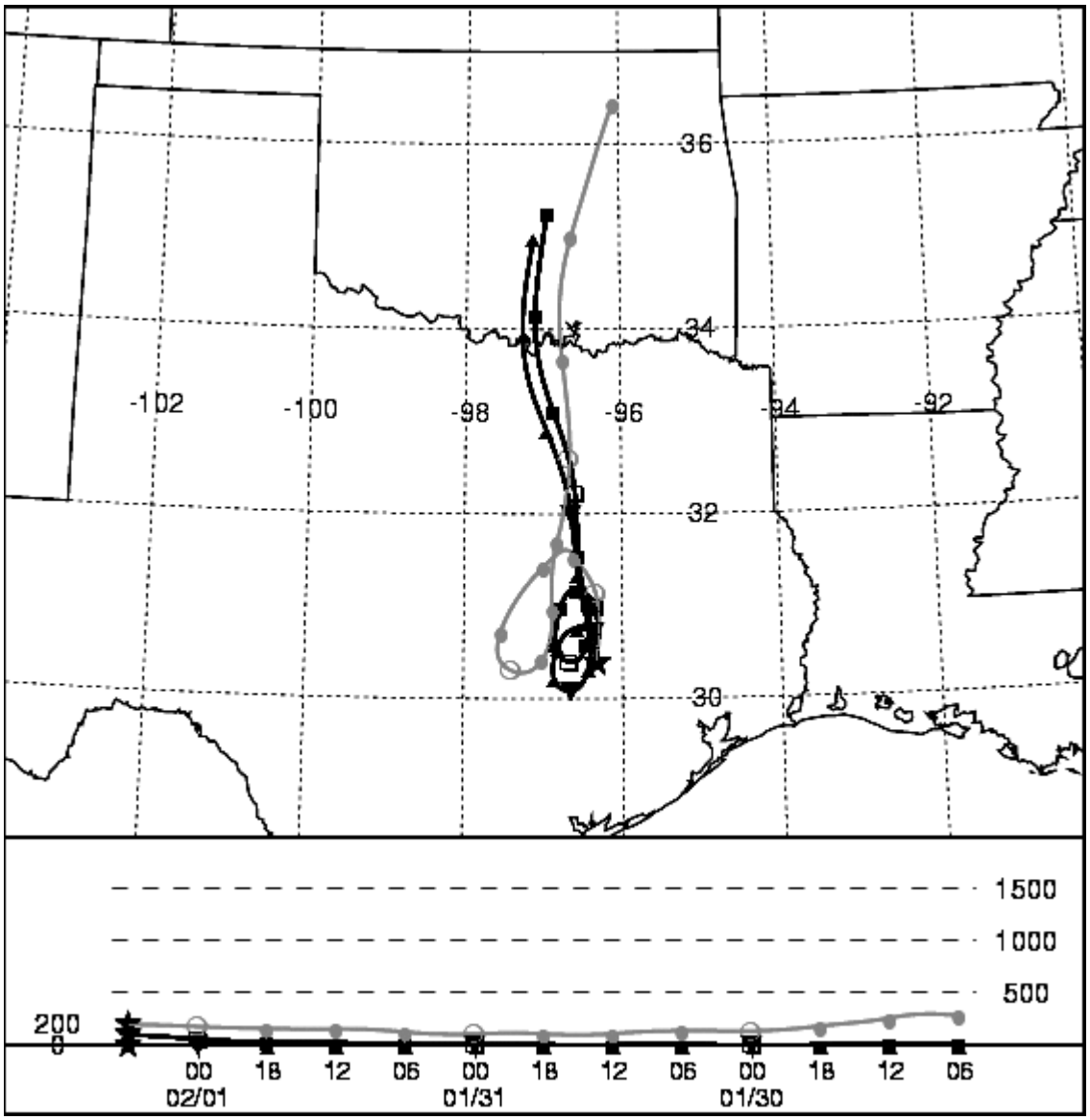

Figure 16. Wind backward trajectories ending on 02/01/2003 at 00:00 in College Station, Texas. Produced with HYSPLIT from the NOAA ARL Website.

Silicon/Silicon Oxide

Ultrafine silicon/silicon oxide aerosol particles, such as those represented in Figure 17, may be generated during silane oxidation. Silanes are artificial gaseous compounds used in the electronic industry for silicon oxide film production [*Azatyan and Kalkanov,* 1980]. Silanes are less stable than alkanes for normal conditions and easily oxidized by atmospheric oxygen. The detection frequency of this aerosol was significantly higher in experiment 2 than in experiments 1 or 3 (Table 3). The main fraction of silicon/silicon oxide particles was detected when the air mass was coming from Houston or its suburbs. Therefore, these particles may have an industrial source in the Houston area. A similar class of silicon/silicon oxide particles dominated the measurements made by RSMS-II during the Houston Supersite experiment [*Phares et al.,* 2003]. The particles described here are larger than those that comprised the silicon class in Houston, and also exhibit ion peaks corresponding to organics, nitrate, and sulfate. These particles may have been coated during transport.

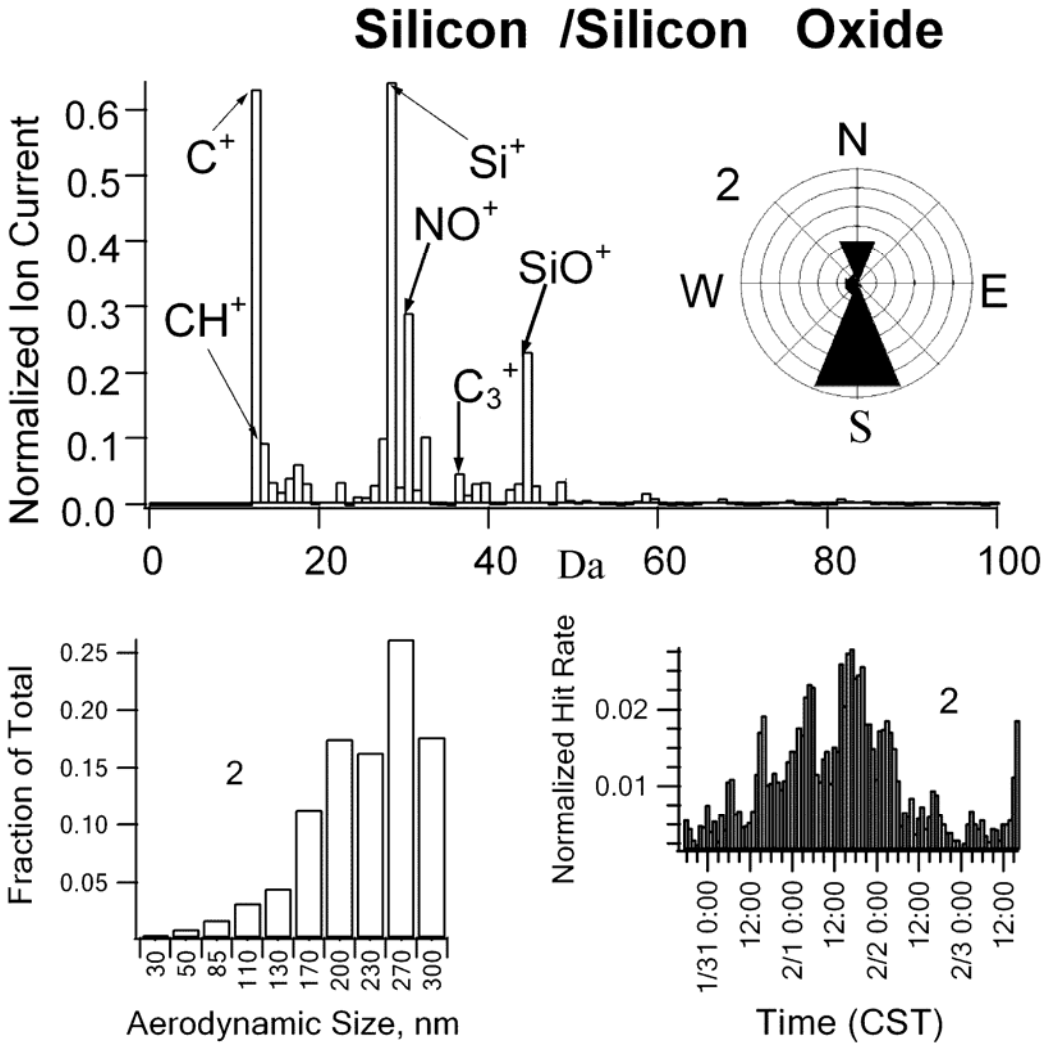

Figure 17. Statistics summary for silicon/silicon oxide compound class.

Calcium/Calcium Oxide

Sixty-four particles exhibiting peaks corresponding to calcium and calcium oxide were detected during experiment 1. The size distribution of this class appears to be shifted towards the coarser mode, as only a small fraction was observed below 200 nm (see Figure 18). A similar particle class was detected during the Houston study [*Phares et al.,* 2003], and was identified to be lime. That particle class was comprised of significantly smaller particles, exhibiting a sharp peak in the size distribution at 70 nm. Another difference with the calcium oxide class observed in the present experiment is that, in addition to the Ca^+ (40 Da) and CaO^+ (56 Da) ion peaks, there are peaks corresponding to C^+ (12 Da), Na^+ (23 Da), Al^+ (27 Da), Si^+ (28 Da), NO^+ (30 Da) (see figure 14). The presence of these ions indicates a more complex particle type, perhaps a natural or artificial calcium alumosilicate.

Particles with such spectra could also originate during Portland cement manufacturing, through pyroprocessing of carbonaceous or other lime-bearing material with silica, alumina and iron oxides [*Soroka*, 1979]. The approximate oxide composition of Portland cement is: CaO 62.8%, SiO_2 21.6%, Al_2O_3 4.6%, Fe_2O_3 2.8%, Na_2O 0.41%, K_2O 0.24%, SO_3 2.1% [*Waddell*, 1989]. There are several cement production plants and shredders in the Dallas, Houston and San Antonio surroundings which may produce calcium-containing particles.

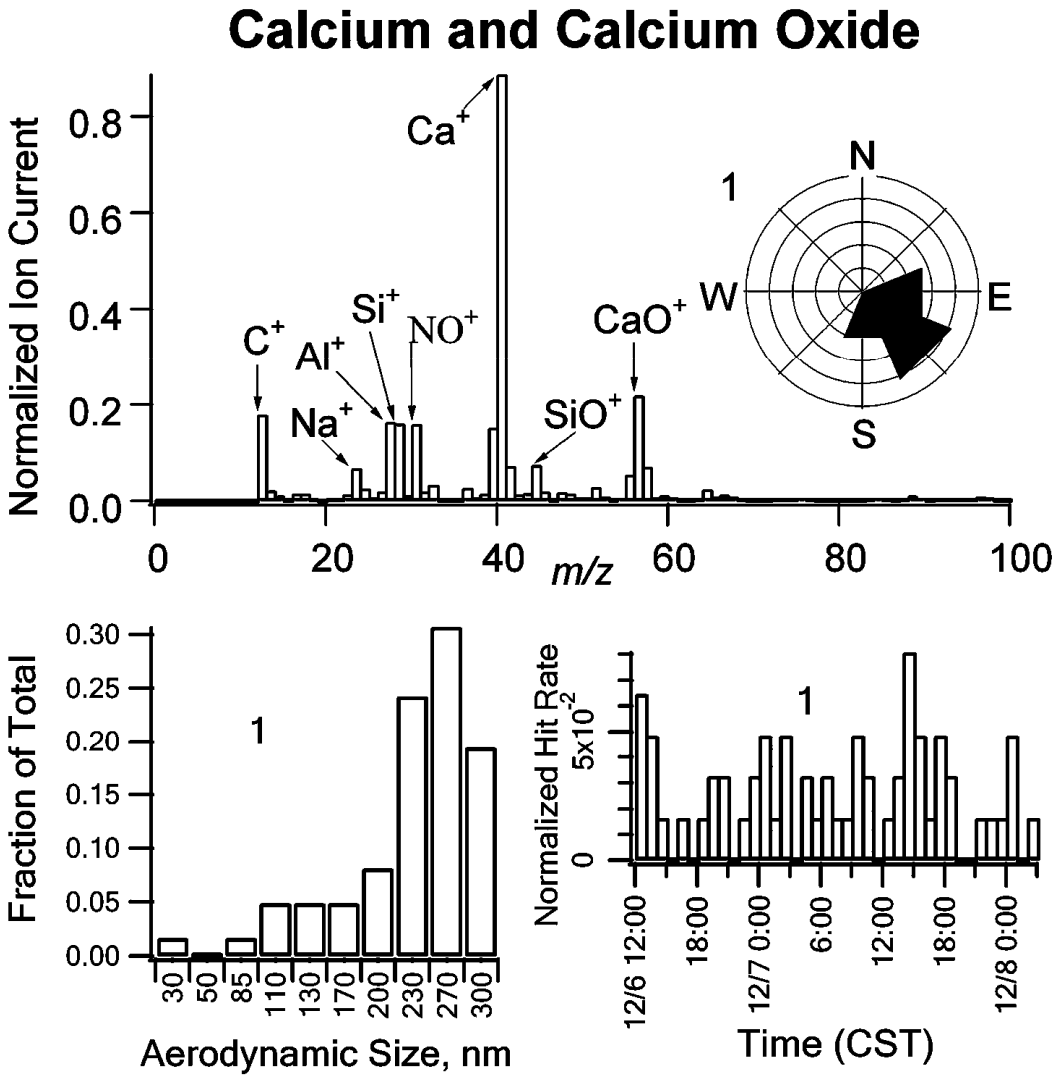

Figure 18. Statistics summary for calcium/calcium oxide compound class.

Aluminum

Figure 19 summarizes a class dominated by an aluminum peak in the mass spectra. Fifty-one aluminum containing particles were detected in experiment 2 and eighty-three in experiment 3. In January, a large fraction of the particles had very small aerodynamic diameters –as small as 30 nm. By contrast, the detected size distribution was shifted to larger sizes in March and no particles smaller than 100 nm were detected.

In addition to the main aluminum peak several other prominent peaks are present, including C^+ (12 Da), Mg^+ (24 Da), Si^+ (28 Da), NO^+ (30 Da), SiO^+ (44 Da), Fe^+ (56 Da) and TiO^+ (64 Da). Such a combination of ions is indicative of bauxite, a heterogeneous geological material composed primarily of aluminum oxide (Al_2O_3), iron oxide (Fe_2O_3) and mixture of various secondary components such as silicon oxide (SiO_2), magnesium oxide (MgO), titanium oxide (TiO_2) and some others [*Milovsky and Kononov.,* 1985]. A major fraction of mined bauxite is used for aluminum production; the rest is used for production of cement, abrasive and refractory materials. There are two aluminum plants in Texas (Alcoa Inc. in Point Comfort and BPU Reynolds Inc. in Corpus Christi) and one aluminum remelting plant (Hydro Aluminum North America, Commerce) [*Plunkert,* 2001]. The maximum detection frequency of aluminum-containing particles occurred at 3:00 am on March 8th. The 96 hour back trajectory determined from the HYSPLIT4 model [*Draxler et al.,* 1988] indicated that particles may have originated at the remelting plant in Commerce, TX (see Figure 20).

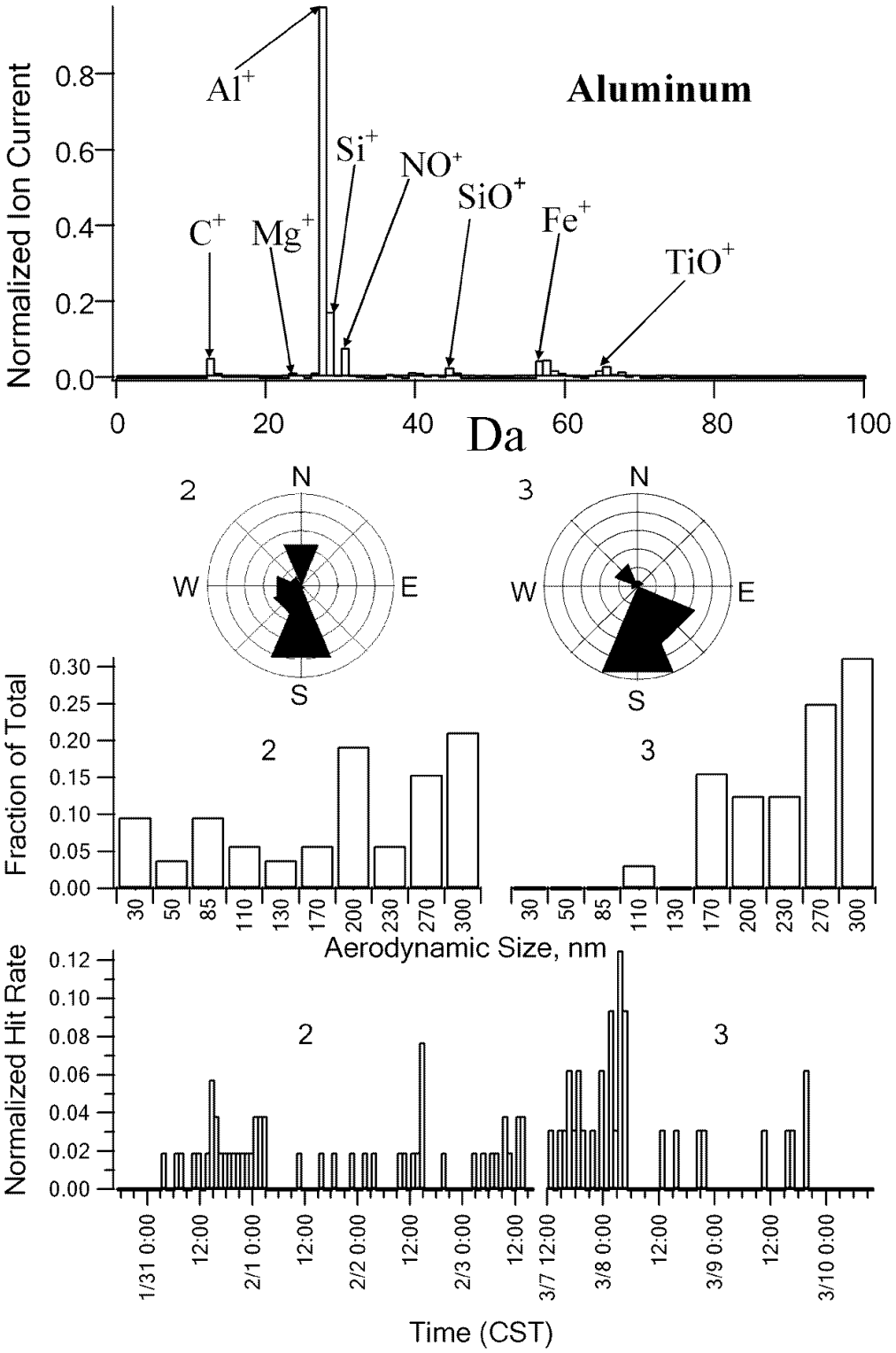

Figure 19. Statistics summary for aluminum compound class.

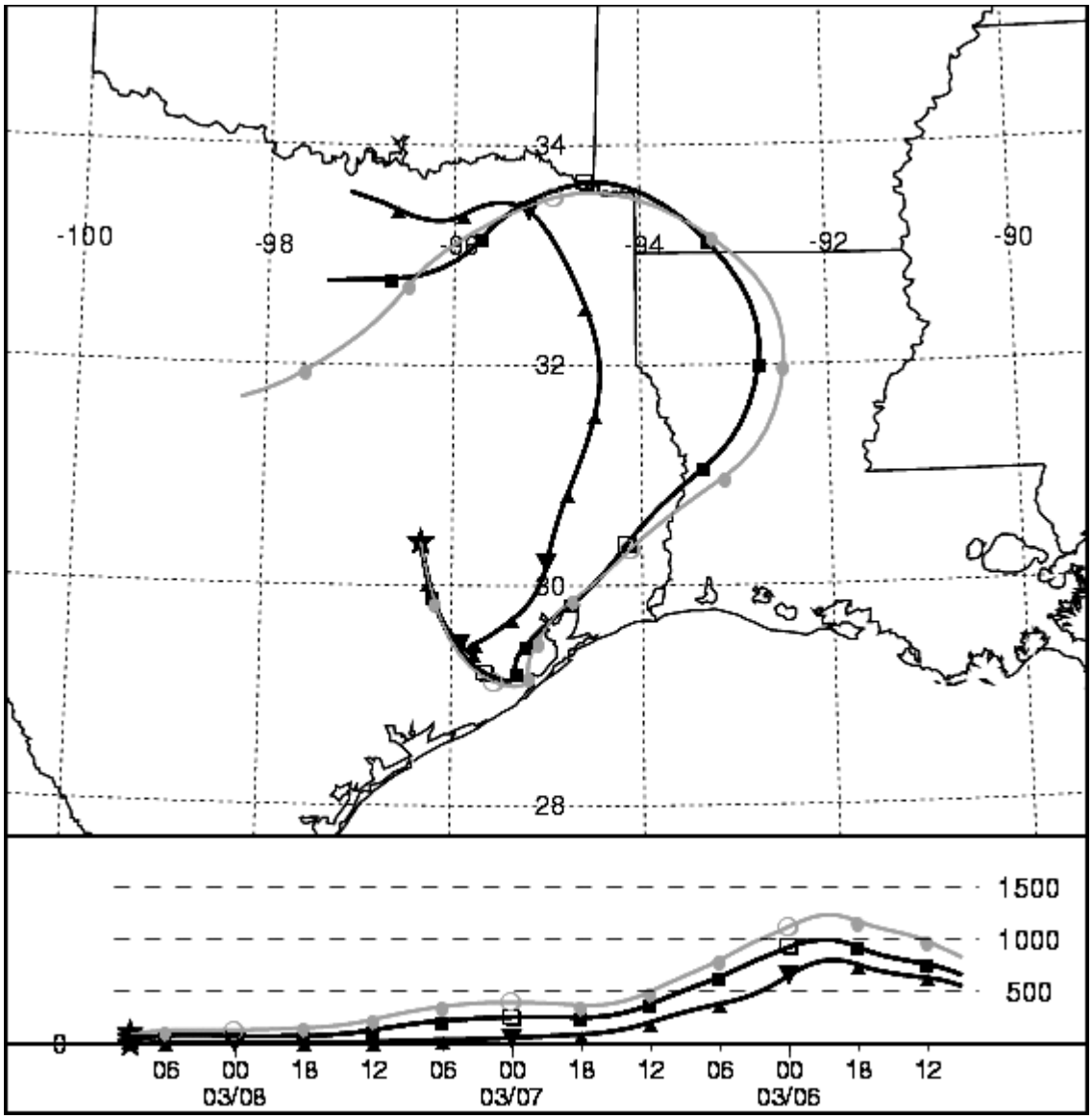

Figure 20. Wind backward trajectories ending on 03/08/2003 at 03:00 in College Station, Texas. Produced with HYSPLIT from the NOAA ARL Website.

Lead

Seventy-four lead containing particles were observed in January (see Figure 21). Although the main sources of the lead are known to be primary and secondary lead smelters [*Spear et al.,* 1998], the presence of the sodium and potassium peaks indicates that this particle type may have originated in a tetraethyl/methyl lead production process. Tetraethyl lead is used as antiknock gasoline additives. It is synthesized by the reaction of the sodium-potassium-lead alloys with the ethyl or methyl chloride. Sodium-potassium-lead alloys can be produced by the electrolysis of chloride–carbonate melts with liquid lead cathode [*Marachevskii et al.,* 1997]. Historically, such alloys were used for the production of tetraethyl lead, an antiknock gasoline additive, by reaction with ethyl or methyl chloride [*Marachevskii et al.,* 1997]. Although tetraethyl lead is no longer produced in North America, lead containing additives are still used for production of high octane number aviation gasoline.

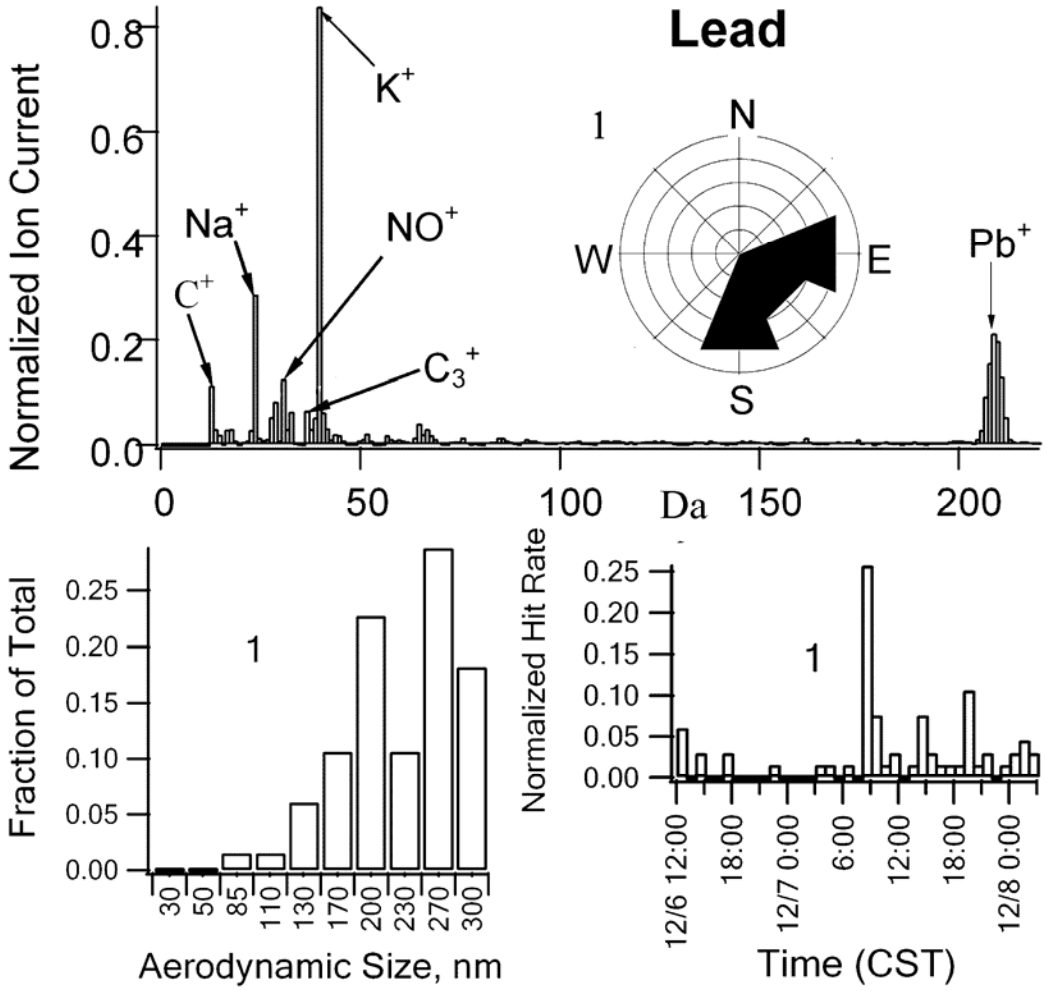

Figure 21. Statistics summary for lead compound class.

Amines

Although large organic molecules tend to fragment during UV laser ablation, some organics, such as dioctylphthalate and pyrene, produce more stable characteristic ion fragments that are readily identifiable [*Phares et al., 2001*]. One class of organics that is easily distinguishable from the main organic classes is the amine class. Amines typically produce prominent ion peaks at 30, 44, 58, 72, and 86 Da, corresponding to fragments that follow the $C_nH_{2n+2}N^+$ pattern [*Phares et al., 2003*]. Amines with fewer than five carbon atoms are generally water-soluble. Primary and secondary amines form strong hydrogen bonds and are highly associated in the liquid state. Simple aliphatic amines are stronger bases than ammonia, and they readily form water–soluble salts with mineral acids [*McMurry, 1986*]. Two types of amines, labeled "amine 1" and "amine 2" and displayed in Figures 22 and 23 were detected in the present study. The heaviest ion cluster detected in Amine 1 corresponds to pentylamine ($C_5H_{12}N^+$); hence the detected amine (or mixture of aliphatic amines) could be soluble in the water. It is possible that this particle may have been coated with nitrate and sulfate, but the NO^+ peak would be masked by the CH_4N^+ peak, and the SO^+ peak, by the C_3^+ peak. This particle type was detected in sufficient amounts only in December. The majority of amine-containing aerosols came from the south with detection maxima at 4:00 pm on February 1st and 2:00 am on February 2nd.

The Amine 2 particle type is characterized by ion peaks at 12, 15, 28, 30, 42 and 58 Da. The presence of the C^+ and CH_3^+ ions suggest an organic particle and the other four peaks resemble the typical Amine pattern, and may thus be identified as CH_2N^+ (28 Da),

CH_4N^+ (30 Da), $C_2H_6N^+$ (42 Da), $C_3H_8N^+$ (58 Da). This particle type was observed only during very short time periods corresponding to the relative humidity minima and temperature maxima (see Figure 18) during all three experiments. We suggest two possible explanations for this observation. First, the aerosol crystallized when the ambient relative humidity dropped below some threshold (crystallization relative humidity), leading to changes in the aerosol ionization properties. One possible amine that could exhibit such a behavior is propilamine-nitrate ($[C_3H_8\text{-}NH_3]$ NO_3), which is water soluble and solid at ambient temperatures. Second, the particle is biogenic in origin, and the gaseous precursors are preferentially emitted during periods of low relative humidity.

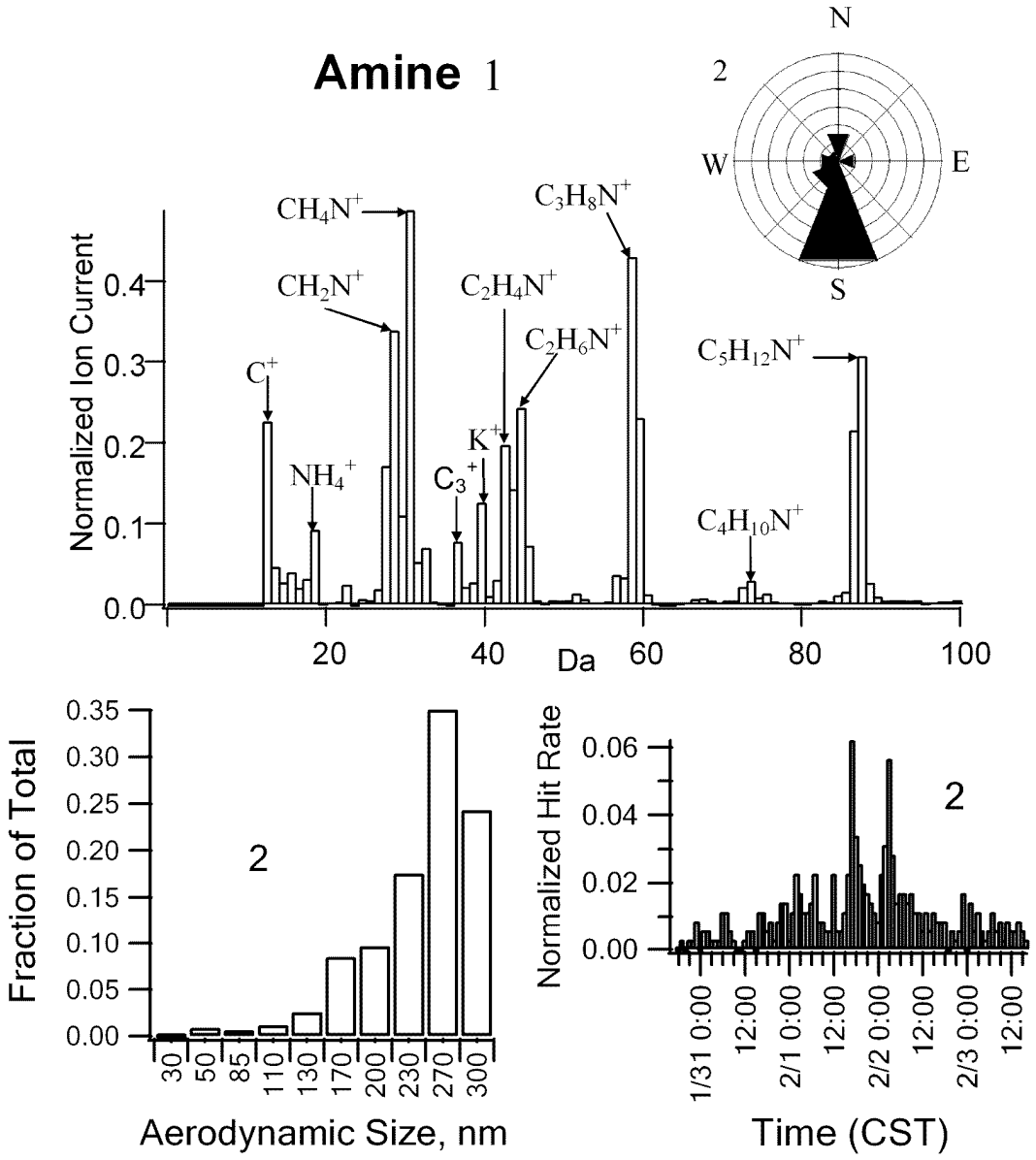

Figure 22. Statistics summary for amine-1 class.

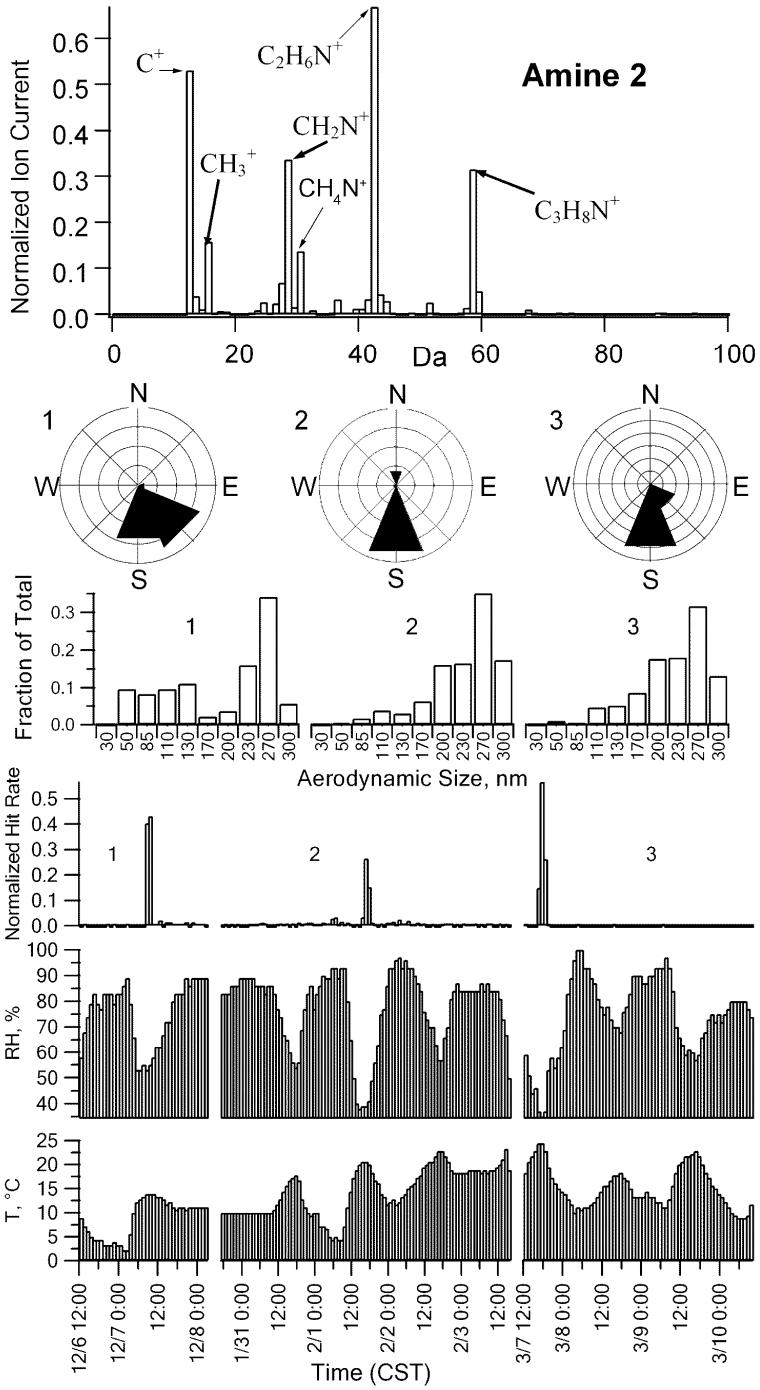

Figure 23. Statistics summary for amine-2 class. Upper graph: average mass spectrum for this class. Polar: Wind rose showing directional preference for this class for each three experiments. Third row from the top: Average size distribution for each experiment. Fourth row: Time distribution of particles detection frequency for each experiment. Fifth row: Relative humidity diurnal variation. Sixth row: Diurnal temperature variation.

CONCLUSION

The single-ultrafine-particle mass spectrometer was shown to be very efficient instrument for the online ambient aerosol characterization. Several improvements were made during the construction period which allowed building of a compact analytical instrument applicable for field experiments. The reflectron type mass spectrometer utilized in the SUPMS design improved quality of the acquired data. The dynamic inlet provided simple and efficient way of the particle size selection and focusing and allowed studying particles as small as 30 nm in diameter. Operation of the instrument's laser at 100 Hz significantly increased particle detection rate which in its turn made it possible to follow rapid changes in atmospheric aerosol properties. The SUPMS is highly automated, easy to operate and requires minimum maintenance. The ability of the SUPMS to collect time and size resolved information about aerosol chemical composition makes it perfect instrument for transport and evolution monitoring of nanoparticles in the atmosphere.

The single-ultrafine-particle mass spectrometer with a very high sampling rate was operated in College Station, TX during the winter of 2002 - 2003. Three separate experiments between December and March were performed. Almost 128,000 particles were detected during 175 hours of sampling. The particle data processed by ART-2a algorithm yielded 15 statistically significant aerosol classes. The average class spectra, size and time distributions were presented graphically.

The aerosol population was dominated by particles containing potassium and carbonaceous characteristic peaks. The carbon and potassium classes were also most

frequently observed classes during the Atlanta and Houston Supersite experiments. These particles classes are considered to be emitted during the fossil fuel and biomass burning processes. Majority of the carbon and potassium spectra collected in College Station in all three experiments contained characteristic nitrate peaks unlike the spectra collected in Atlanta and Houston. Presence of the NO^+ signals in the particles spectra indicated that the particles could be covered by ammonia nitrate coating during the aerosol transport through the areas with a high level of agricultural activity. Furthermore, the nitrate, potassium/nitrate and carbon/nitrate classes combined together represented the most commonly observed class during all three experiments. The high nitrate content classes exhibited similar time, wind and size distributions different from the distributions of the corresponding classes with low nitrate content. The concentration of the nitrate-containing particles was found to be a strong function of temperature and relative humidity through the March experiment. A simple thermodynamic analysis showed that the abundance of the nitrate containing particles is inversely proportional to the ammonia nitrate dissociation constant. It was also shown that these particles could be in a liquid phase during the high relative humidity periods.

The silicon/silicon oxide class is one of the dominant classes detected in January. Similar particles were detected by the RSMS-II during the Houston Supersite experiment and could have possible source in a Houston industrial area. The size distribution of the silicon particles detected in College Station is shifted to a coarse mode. Presence of the organic and nitrate characteristic peaks indicated that these particles may have been coated during the transport.

Minor classes observed during the College Station campaign included: vanadium, iron, calcium, aluminum, lead, sea salt, amine 1 and 2 classes. The vanadium, calcium, aluminum and lead classes are most likely to have industrial sources. Similar aerosol classes were observed by the RSMA-II instrument during the previous experiments in the big industrial centers such as Houston and Atlanta.

The vanadium class particles were released in a process of crude oil thermal cracking or heavy fuel combustion. Major source of these particle types was found to be Houston petroleum refining industry. Presence of the nitrate characteristic peak in the ion spectrum indicates that the particles were coated during the aerosol transport from Houston to College Station.

The iron class comprised less than one percent of the total number of particles analyzed in College Station. The iron particles were probably brought from the distant pig iron/steel production plants, or coal-fired power plants.

The calcium/calcium oxide particles were detected only during the third experiment. Presence of the ionic groups corresponding to the calcium, calcium oxide, carbon, sodium, aluminum, silicon and nitrate indicates a natural or artificial calcium alumosilicate. Particles with such elemental composition could have originated during Portland cement manufacturing at one of the cement production plants located in Dallas, Houston or San Antonio.

The aluminum type particles were detected in significant amounts only during January and March experiments. The unique combination of the carbon, magnesium, silicon, silicon oxide, iron and titanium oxide peaks is an indicative of the bauxite,

geological material used for alumina production. The HYSPLIT4 wind back trajectory simulation showed that such particle type may have originated at the aluminum remelting plant in Commerce, TX.

More than seventy lead containing particles were detected in January. The possible sources of the lead class aerosol are lead remelting plants located in Texas.

The sea salt particles comprised roughly one percent of the total aerosol collected. The characteristic nitrate peak resulted probably from the partial substitution of chlorine with the nitrate ion. Majority of the sea salt particles came from the Gulf of Mexico direction, but some fraction of them came from North in January and March as a result of a large recirculation of the air masses over eastern Texas.

Two amine classes detected during the College Station experiment were evidenced by the prominent ion peaks which are following the $C_nH_{2n+2}N^+$ pattern. The heaviest ion cluster corresponds to $C_5H_{12}N^+$ for the amine 1 class and $C_3H_8N^+$ for the amine 2. The amine 1 particles were detected in sufficient amounts only in December. The amine 2 particles were detected in all three experiments but only during very short time periods corresponding to the relative humidity minima and temperature maxima. Two possible explanations for the amine 2 class behavior were made. First, the aerosol changes its ionization properties when relative humidity drops below crystallization relative humidity. Second, the particles have biogenic gaseous precursors emitted only during periods of low relative humidity.

The ultrafine ambient aerosol in College Station was found to be influenced by transport from the major Texas urban centers and by local agricultural activity. Major

aerosol classes were similar to the aerosol classes observed by the RSMS-II during the Houston Supersite experiment and in some cases could have the same sources. Data collected by the SUPMS coupled with the HYSPLIT technique was used for the possible source allocation. Particle time distributions were found to be non uniform. Several aerosol classes were detected only in one or two experiments. The average aerosol size distributions in College Station were shifted to the fine mode in contrast to Houston where a large fraction of particles was detected in the ultrafine mode. The aerosol size distribution and presence of the characteristic nitrate signal in the majority of particle spectra observed in College Station is an indication of the important role of the ammonia nitrate in the process of the aerosol aging in the rural area. Time distributions of several classes were found to be a function of meteorological conditions.

REFERENCES

Azatyan V. V. and V. A. Kalkanov, Mechanism of silane oxidation, *Reaction Kinetics and Catalysis Letters, 15* (3), 367-372, 1980.

Carson P. G., M. V. Johnston and A. S. Wexler, Laser desorption/ionization of ultrafine aerosol particles, *Rapid Communications in Mass Spectrometry, 11*, 993-996, 1997.

Cziczo D. J., D. M. Murphy, D. S. Thomson, Composition of individual particles in the wakes of an Athena II rocket and the space shuttle, *Geophysical Research Letters, 29* (21), 331-334, 2002.

Gard E. E., J. E. Mayer, B. D. Morrical, R. Dienes, D. P Fergenson, and K. A. Prather, Real-time analysis of individual atmospheric aerosol particles: Design and performance of a portable ATOFMS, *Anal. Chem., 69*, 4083-4091, 1997.

Gard E. E., M. J. Kleeman, D. S. Gross, L. S. Hughes, J. O. Allen, B. D. Morrical, D. P Fergenson, T. Dienes, M. E. Galli, R.J. Johnson, G. R. Cass, and K. A. Prather, Direct observation of heterogeneous chemistry in the atmosphere, *Science, 279*, 1184-1187, 1998.

Gasparini R., R. Li and Collins D. R., Integration of size distributions and size-resolved hygroscopicity measured during the Houston Supersite for compositional categorization of the aerosol, *Atmospheric Environment*, *38* (20), 3285-3303, 2004.

Guazzotti S. A., K. R. Coffee and K. A. Prather, Real time monitoring of size-resolved single particle chemistry during INDOEX-IFP 99, *Journal of Aerosol Science, 31*, S182-S183, 2000.

Dahneke B. E., and H. Flachsbart, An aerosol beam spectrometer, *Journal of Aerosol Science, 3*, 345-349, 1972.

Dahneke B. E., Y. S. Cheng, Properties of continuum source particle beams. I. Calculation methods and results, *Journal of Aerosol Science, 10*, 257-274, 1979.

Das R. and D. J. Phares, Expansion of an ultrafine aerosol through a thin-plate orifice, *Journal of Aerosol Science, in press*, 2004.

Draxler R. R., Hybrid single-particle Lagrangian integrated trajectories (HY-SPLIT): model description, *NOAA Technical Memorandum, ERL ARL – 166*, 1988.

Fernandez de la Mora and P. Riesco-Chueca, Aerodynamic focusing of particles in a carrier gas, *Journal of Fluid Mechanics, 195*, 1-21, 1988.

Hughes L. S., J. O. Allen, M. J. Kleeman, R. J. Johnson, G. R. Cass, D. S. Gross, E. E. Gard, M. E. Galli, B. D. Morrical, D. P. Fergenson, T. Dienes, C. A. Noble, D. Liu, P. J. Silva and K. A. Prather, Size and composition of atmospheric particles in southern California, *Environmental Science and Technology, 33*, 3506-3515, 1999.

Israel G. W. and S. K. Friedlander, High-speed beams of small particles, *Journal of Colloid and Interface Science, 24*, 330-337, 1967.

Jayne J. T, D. C. Leard, X. Zhang, P. Davidovits, K. A. Smith, C. E. Kolb, and D. R. Worsnop, Development of an aerosol mass spectrometer for size and composition analysis of submicron particles, *Aerosol Science and Technology 33*, 49-70, 2000.

Jimenez J. L., J. T. Jayne, Q. Shi, C. E. Kolb, D. R. Worsnop, I. Yourshaw, J. H. Seinfeld, R. C. Flagan, X. Zhang, K. A. Smith, J. W. Morris and P. Davidovits, Ambient aerosol sampling using the aerodyne Aerosol Mass Spectrometer, *Journal of Geophysical Research, 108* (D7)*,* 8425, 2003.

Johnston M. V., Sampling and analysis of individual particles by aerosol mass spectrometry, *Journal of Mass Spectrometry, 35*, 585-595, 2000.

Kane D. B. and M. V. Johnston, Size and composition biases on the detection of individual ultrafine particles by aerosol mass spectrometry, *Environmental Science and Technology, 34*, 4887-4893, 2000.

Lake D. A., M. P. Tolocka, M. V. Johnston and A. S. Wexler, Mass Spectrometry of individual particles between 50 and 750 nm in diameter at the Baltimore Supersite, *Environmental Science and Technology, 37*, 3268-3274 2003.

Liu D. Y., D. Rutherford, M. Kinsey and K. A. Prather, Real-time monitoring of pyrotechnically derived aerosol particles in the troposphere, *Analytical Chemistry, 69*, 1808-1814, 1997.

Liu D. Y., K. A. Prather, and S. V. Hering, Variation in the size and chemical composition of nitrate-containing particles in Riverside, CA, *Aerosol Science and Technology 33,* 71-86, 2000.

Liu D. Y., R. J. Wenzel., and K. A. Prather, Aerosol time-of-flight mass spectrometry during the Atlanta Supersite experiment: 1. Measurements, *Journal of Geophysical Research, 108* (D7), 8426, 2003.

Mallina R. V., A. S. Wexler, K. P. Rhoads and M. V. Johnston, High speed particle beam generation: a dynamic focusing mechanism for selecting ultrafine particles, *Aerosol Science and Technology 33*, 87-104, 2000.

Marachevskii A. G., Calculation of density and excessive molar volume of liquid sodium-lead-potassium alloys, *Russian Journal of Applied Chemistry, 70* (1), 36-40, 1997.

McMurry J., *Fundamentals of Organic Chemistry*., Brooks/Cole Publishing Company, Pacific Grove, California, 1986.

Middlebrook A. M., D. M. Murphy and D. S. Thomson, Observation of organic material in individual maritime particles at Cape Grim during the First Aerosol Characterization Experiment (ACE 1), *Journal of Geophysical Research, 103* (D13), 16475-16483, 1998.

Middlebrook A. M., D. M. Murphy, S. H. Lee, D. S. Thomson, K. A. Prather, R. J. Wenzel, D. Y. Liu, D. J. Phares, K. P. Rhoads, A. S. Wexler, M. V. Johnston, J. L. Jimenez, J. T. Jayne, D. R. Worsnop, I. Yourshaw, J. H. Seinfeld, and R. C. Flagan, A comparison of particle mass spectrometers during the 1999 Atlanta Supersite Project, *Journal of Geophysical Research-Atmospheres, 108* (D7), 8424, 2003.

Milovsky A. V. and Kononov O. V., *Mineralogy*, translated from the Russian by G. G. Egorov, Mir Publishers, Moscow, 1985.

Misselbrook T. N., T. J. Van der Weerden, B. F. Pain, S. C. Jarvis, B. J. Chambers, K. A. Smith, V. R. Phillips, and T. G. M. Demmers, Ammonia emission factors for UK agriculture, *Atmospheric Environment, 34* (6), 871-880, 2000.

Murphy D. M. and D.S. Thompson, Chemical composition of single aerosol particles at Idaho Hill: Positive ion measurements, *Journal of Geophysical Research, 102* (D5), 6341-6352, 1997a.

Murphy D. M. and D. S. Thompson, Chemical composition of single aerosol particles at Idaho Hill: Negative ion measurements, *Journal of Geophysical Research, 102* (D5), 6353-6368, 1997b.

Murphy D. M., D. S. Thompson and A. M. Middlebrook, Bromine, iodine, and chlorine in single aerosol particles at Cape Grim, *Geophysical Research Letters, 24*, 3197-3200, 1997c.

Murphy D. M., D. S. Thompson and M. J. Mahoney, In situ measurements of organic, meteoritic material, mercury, and other elements in aerosol at 5 to 19 kilometers, *Science, 282*, 1664-1669, 1998a.

Murphy D. M., D. S. Thompson, A. M. Middlebrook and M. E. Schein, In situ single-particle characterization at Cape Grim, *Journal of Geophysical Research, 103* (D13), 16485-16491, 1998b.

Noble C. A. and K. A. Prather, Real-time measurements of correlated size and composition profiles of individual atmospheric aerosol particles, *Environmental Science and Technology, 30,* 2667-2680, 1996.

Noble C. A and K. A. Prather, Real-time single particles monitoring of a relative increase on marine aerosol concentration during winter rainstorms, *Geophysical Research Letters, 24,* 2753-2756, 1997.

Pastor S. H., J. O. Allen, L. S. Hughes, Prakash Bhave, G. R. Cass and K. A. Prather, Ambient single particle analysis in Riverside, California by aerosol time-of-flight mass spectrometry during the SCOS97-NARSTO, *Atmospheric Environment, 37,* S239-S258, 2003.

Phares D. J., K. P. Rhoads and A. S. Wexler, Application of the ART-2a algorithm to laser ablation aerosol mass spectrometry of particle standards, *Anal. Chem., 73,* 2338-2344, 2001.

Phares D. J., K. P. Rhoads and A. S. Wexler, Performance of a single ultrafine particle mass spectrometer, *Aerosol Science and Technology, 36,* 583-592, 2002.

Phares D. J., K. P. Roads, M. V. Johnston and A. S. Wexler, Size-resolved ultrafine particle composition analysis. 2. Houston, *Journal of Geophysical Research, 108* (D7)*,* 8420, 2003.

Plunkert P. A., *Bauxite and Alumina,* U.S. Department of the Interior, Reston, Virginia, 2001.

Rhoads K. P., D. J. Phares, A. S. Wexler and M. V. Johnston, Size-resolved ultrafine particle composition analysis. 1. Atlanta, *Journal of Geophysical Research, 108* (D7)*,* 8418, 2003.

Schneider J., S. Borrmann, A. G. Wollny, M. Bläsner, N. Mihalopoulos, K. Oikonomou, J. Sciare, A. Teller, Z. Levin and D. R. Worsnop, Online mass spectrometric aerosol measurements during the MINOS campaign (Crete, August 2001), *Atmospheric Chemistry and Physics, 4,* 65-80, 2004.

Schwartz M. H. and R. P. Andres, Theoretical basis of the time-of-flight aerosol spectrometer: a method for monitoring the size distribution of submicron aerosol particles, *Journal of Aerosol Science, 7,* 281-296, 1976.

Smith K. R., J. M. Veranth, J. S. Lighty and A. E. Aust, Mobilization of iron from coal fly ash was dependent upon the particle size and the source of coal, *Chemical Research Toxicology, 11 (12),* 1494-1500, 1998.

Soroka I., *Portland cement paste and concrete*, The Macmillan Press LTD, London 1979.

Spear T. M., M. A. Werner, J. Bootland, E. Murray, G. Ramachandran and J. H. Vincent, Assessment of particle distribution of health-relevant aerosol exposures of primary lead smelter workers, *Annals of Occupational Hygiene, 42* (2)*,* 73-80, 1998.

Stelson A. W. and J. H. Seinfeld, Relative humidity and temperature dependence of the ammonium nitrate dissociation constant, *Atmospheric Environment, 16,* 983-993, 1982.

Thompson D. S. and D. M. Murphy, Laser-induced ion formation thresholds of aerosol particles in vacuum, *Applied Optics, 32* (33)*,* 6818-6826, 1993.

Thompson D. S., A. M. Middlebrook, and D. M. Murphy, Thresholds for laser-induced ion formation from aerosol in a vacuum using ultraviolet and vacuum-ultraviolet laser wavelengths, *Aerosol Science and Technology, 26*, 544-559, 1997.

Thompson D. S., M. E. Schein, and D. M. Murphy, Particle analysis by laser mass spectrometry WB-57F instrument overview, *Aerosol Science and Technology, 33,* 153-169, 2000.

Trimborn A., K. P. Hinz and B. Spengler, Online analysis of atmospheric particles with a transportable laser mass spectrometer, *Aerosol Science and Technology, 33,* 191-201, 2000.

Trimborn A., K. P. Hinz and B. Spengler, Online analysis of atmospheric particles with a transportable laser mass spectrometer during LACE 98, *Journal of Geophysical Research, 107* (D21)*,* 8132, 2002.

Vogt R., U. Kirchner, V. Scheer, K. P. Hinz, A. Trimborn and B. Spengler, Identification of diesel exhaust particles at an Autobahn, urban and rural location using single-particle mass spectrometry, *Aerosol Science, 34,* 319-337, 2003.

Waddell J. J., *Concrete Manual,* International Conference of Building Officials, Whittier, California, 1989.

Weber R. J., D. Orsini, Y. Daun, Y.-N. Lee, P. J. Klotz and A. Brechtel, A particles-into-liquid collector for rapid measurement of aerosol bulk chemical composition, *Aerosol Science and Technology, 35,* 718-727, 2001.

Weinberg E. D., The development of awareness of the carcinogenic hazard of inhaled iron, *Oncology Research, 11* (3)*,* 109-113, 1999.

Zhang X.Y., R. Arimoto, G. H. Zhu, T. Chen and G. Y. Zhang, Concentration, size-distribution and deposition of mineral aerosol over Chinese desert regions., *Tellus Series B-Chemical and Physical Meteorology, 50* (4), 317-330, 1998.

VITA

Stanislav Y. Glagolenko was born on 21st of May, 1978, in Chelyabinsk-65, Russia, to Mr. U.V. Glagolenko and Mrs. T.G. Glagolenko. He graduated with a Chemical Engineer diploma from the Mendeleyev University of Chemical Technology of Russia in March 2001. In 2000-2001 he worked as a laboratory assistant in the Laboratory of Chromatography and Sorption of Radioactive Elements, Institute of Physical Chemistry, Russian Academy of Sciences, Moscow, Russia. He attended Texas A&M University from August 2001 to August 2004, where he received his Master of Science degree in Mechanical Engineering. He can be reached at 19-257 Prospect 60-Letiya Oktyabrya, Moscow, 117036, Russia. E-mail: glagoliki@hotmail.com